SINGLE PHOTON DETECTION WITH SILICON-BASED AVALANCHE PHOTODIODE

A Thesis

by

Burcu Yerli

Submitted to the
Graduate School of Sciences and Engineering
in Partial Fulfillment of the Requirements for
the Degree of

Master of Science

in the
Department of Electrical and Electronics Engineering

Özyeğin University
January 2024

SINGLE PHOTON DETECTION WITH SILICON-BASED AVALANCHE PHOTODIODE

Approved by:

Asst. Prof. Kadir Durak, Advisor
Dept. of Electrical & Electronics Eng.
Özyeğin University

Asst. Prof. Göktürk Poyrazoğlu
Dept. of Electrical & Electronics Eng.
Özyeğin University

Prof. Dr. Ali Bozbey
Dept. of Electrical & Electronics Eng.
TOBB University of Economics and Technology

Date Approved: January 4, 2024

To ones I love...

ABSTRACT

Due to significant advances in quantum technologies, the use of single photon detectors (SPDs) is becoming common in various fields. As a result of the excellent photodetection performance of SPDs, they are used in a wide range of fields, such as quantum cryptography, astronomy, spectroscopy, and medical applications. There is no doubt that improvements in the performance of SPDs will pave the way for new technologies based on quantum information. Over the years, several different types of SPDs have been developed, such as photomultiplier tubes based on vacuum tubes, avalanche photodiodes (APDs) based on semiconductors, or nanowires based on superconducting technology. Any of these technologies have been preferred by evaluating their advantages and disadvantages for the intended applications. At that point, SPDs based on semiconductor technology have many advantages, including low voltage operation, high reliability, simple electronic requirements, and high detection efficiency. In this work, the TO-8 SAP500 series Silicon APD provided by Laser Component was preferred, the driving circuit was designed for visible (VIS) range sensing applications, and all stages of work were explained in detail. This thesis consists of four sections: the general information on SPDs is covered in the first section, the general information on APDs is covered in the second section, the experimental part is covered in the third section, and the results are covered in the last section.

ÖZETÇE

Kuantum teknolojilerindeki önemli gelişmeler nedeniyle, tek foton dedektörlerinin (TFD'ler) kullanımı çeşitli alanlarda yaygınlaşmaktadır. TFD'ler, mükemmel ışık algılama performansları sonucunda; kuantum kriptografi, astronomi, spektroskopi ve tıbbi uygulamalar gibi çok çeşitli alanlarda kullanılmaktadırlar. TFD'lerin performansındaki gelişmelerin, kuantum bilgiye dayalı yeni teknolojilerin önünü açacağına hiç şüphe yoktur. Yıllar içinde, vakum tüplerine dayalı fotoçoğaltıcı tüpler, yarı iletkenlere dayalı çığ fotodiyotları (ÇFD) ve süper iletken teknolojisine dayalı nanoteller gibi birkaç farklı TFD türü geliştirilmiştir. Bu teknolojilerden herhangi biri amaçlanan uygulamalara yönelik avantaj ve dezavantajları değerlendirilerek tercih edilmektedir. Bu noktada, yarı iletken teknolojisine dayalı TFD'lerin düşük voltajda çalışma, yüksek güvenilirlik, basit elektronik gereksinimler ve yüksek algılama verimliliği gibi birçok avantajı vardır. Bu çalışmada Laser Component firmasının sağladığı TO-8 SAP500 serisi Silicon ÇFD tercih edilmiş olup, görünür bölge algılama uygulamaları için sürücü devresi tasarlanmış ve tüm aşamalar detaylı bir biçimde açıklanmıştır. Bu tez dört bölümden oluşmaktadır: birinci bölümde TFD'ler hakkında genel bilgiler, ikinci bölümde ÇFD'ler hakkında genel bilgiler, üçüncü bölümde deneysel kısım ve son bölümde ise sonuçlar yer almaktadır.

ACKNOWLEDGEMENTS

First of all, I would like to thank my supervisor, Asst. Prof. Kadir Durak, for giving me the opportunity to meet with the wonderful working area and his support.

I would like to express my special thanks to my colleagues Hatun and Adil from TUBITAK BILGEM for their mentoring and motivation.

To Can and Alper, thank you for always answering my questions with their patience and always sharing with me their knowledge with all their humility. With their help, overcoming all the challenges would be much easier.

I would like to thank you, Ali Soner, for guiding and contributing to our work with his kindness.

I would like to thank the special people in the Embedded Systems and Digital Design Department at TUBITAK BILGEM for being wonderful colleagues and friends.

Lastly, I would like to thank my loved ones for supporting me and believing in me.

I acknowledge the support of The Scientific and Technological Research Council of Türkiye (TUBITAK).

TABLE OF CONTENTS

LIST OF TABLES

LIST OF FIGURES

CHAPTER I

INTRODUCTION

Since photons are relatively easy to produce, control, and detect, most quantum information and communication experiments have focused on studying photonic state manipulation [1]. Such experimental investigations require single photon detection in the desired wavelength range, depending on the application. As a result, using SPDs in various fields, from medical applications to industry, is becoming increasingly familiar with the emerging quantum information. SPDs, which many companies commercially offer, are critical as they are an essential export item and lead many new technologies. They have been utilized in a variety of fields such as single-molecule detection [2], astronomy [3], fluorescence lifetime imaging [4], diffuse optical tomography [5], Förster resonance energy transfer (FRET) for studying protein folding [6], spectroscopy [7], remote sensing [8], the detection of bioluminescence [9], ultra-low voltage Time-Resolved Emission (TRE) measurements of Very Large Scale Integration (VLSI) circuits [10], underwater wireless optical communication [11] and DNA sequencing [12]. Improvements in the performance of these detectors will open the path for the development and implementation of innovative technologies across diverse industries.

The growing interest in SPDs is evidenced by the rapid increase in the number of research articles and scientific studies dedicated to unraveling their potential. This increase in academic interest underscores the profound impact of these detectors on the scientific community and industry. Researchers, driven by an insatiable curiosity and the recognition of the transformative capabilities of SPDs, have propelled these detectors to the forefront of scientific exploration. The remarkable sensitivity and

precision of SPDs have not only redefined the boundaries of what is experimentally feasible but have also fueled an ever-expanding quest for innovation and discovery. The trend, as illustrated in Figure 1 with results up to 2023, unmistakably signifies the ongoing and escalating interest in SPDs. As technological advancements continue, the evolving landscape of SPD research promises not only to deepen our understanding of fundamental physics but also to catalyze breakthroughs in a diverse array of scientific and technological domains.

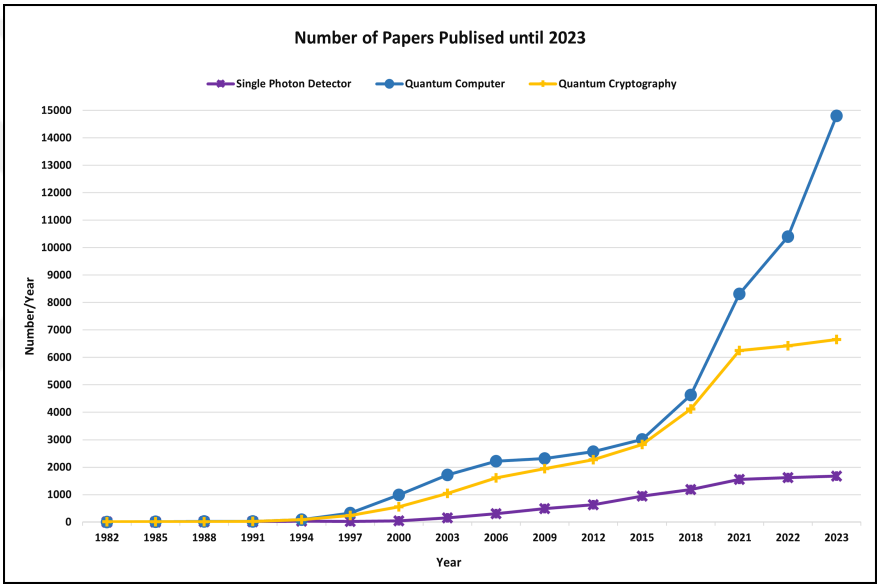

Figure 1: Papers published by 2023. Google Scholar search terms are shown.

1.1 A Short History of Single Photon Detectors

Over the years, several different types of SPDs have been developed, such as photomultiplier tubes (PMTs) based on vacuum tubes, APDs based on semiconductors, or nanowires based on superconducting technology [13]. PMTs are known as the first single photon detectors capable of detecting light with very low intensity. These detectors detect the single photon by multiplying the current generated by incoming

light in many dynodes. The invention of the PMT results from two main achievements: the photoelectric effect and the secondary emission [14]. Heinrich Hertz utilized ultraviolet light to demonstrate the first photoelectric effect in 1887 [15]. Two years later, Elster and Geitel confirmed the same result using VIS light striking alkali metals [16] and developed what evolved into the photoelectric cell [17]. However, it was not possible to see the signal from a single photon until the invention of the electron multiplier [18]. In 1930, Soviet-Russian physicist and engineer Leonid Aleksandrovitch Kubetsky proposed a device that combined photocathodes and dynodes, or secondary electron emitters, inside a single tube [19]. Then, the first PMT became 1936 a commercial product. Figure 2 shows the first PMT, which is called Kopitsky's tube. Although they are highly sensitive in the ultraviolet, VIS, and near-infrared ranges, they have disadvantages such as high sensitivity to magnetic fields and high price due to the complex mechanical design inside the vacuum container [20]. These disadvantages led to the need to find an alternative to PMT.

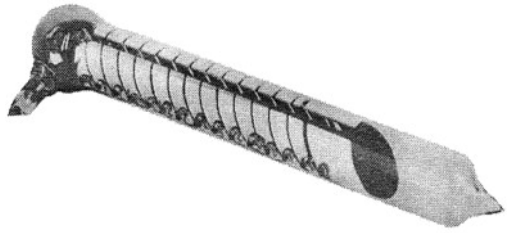

Figure 2: The first photomultiplier tube (Kubetsky's tube) [19].

The PIN photodiode, which Jun-Ichi Nishizawa and his colleagues invented in 1950 [21], was used in essential physics studies that require a high magnetic field. However, because the device has no internal gain, detecting lower light with high efficiency was difficult with PIN diodes [20]. Consequently, there was a need to find new technologies for such applications. In the mid-1960s, the development of solid-state optical single-photon detection was done by McIntyre's [22] and Haitz's work [23] on Geiger-mode APDs [20]. The illustration shown in Figure 3 represents McIntyre's

model structure of Silicon (Si) APD.

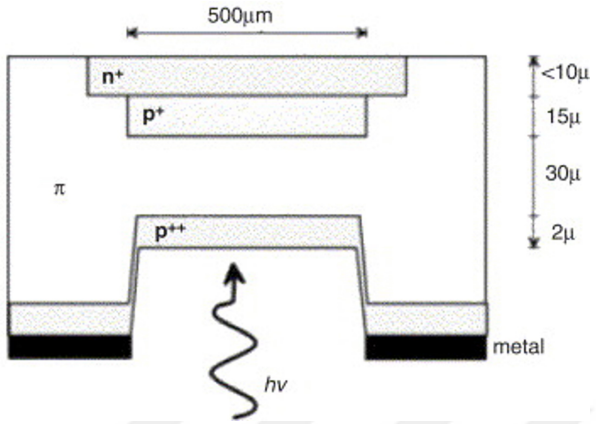

Figure 3: The first APD made by McIntyre [20].

Thanks to the photoelectric effect, APDs are highly sensitive semiconductor detectors that can convert light into an electrical signal [24]. This technology is utilized with two modes: linear mode, which is biased slightly below the breakdown voltage, and Geiger mode, which is biased well above the breakdown voltage. In linear mode, the detection of single photons is feasible; however, it is not practical and effective because their gain is low, and they are affected by strong excess noise. Instead, in Geiger mode, a single electron-hole pair generation can start an avalanche current in the milliampere range since the electric field in the depletion layer is so strong at reverse bias [25]. Thus, the detection of single photons with APDs used in Geiger mode has become possible with high efficiency and low noise. However, not all APDs are convenient for detecting single photons [1]. When APDs are particularly developed to work as single-photon detectors, they are called single photon avalanche diodes (SPADs) with special semiconductor structures [26]. The increasing interest in research in quantum information over the years has led to increased research on SPADs [27]. Today, there are various types of commercially available SPADs based on different technologies in the market, and they offer a diverse range of applications. On the other hand, SPAD development is much more challenging in the infrared (IR) range because of the need for special materials such as low noise and good absorption

for IR [18]. As a result, IR SPADs are inferior to Si SPADs in all features; however, several studies have been conducted on this issue [28].

In recent years, studies have focused on superconducting nanowire single photon detectors (SNSPDs) due to their advantages, such as high efficiency, low dark counts, and excellent timing resolution [29]. In 1911, superconductivity was discovered by the Dutch physicist Heike Kamerlingh Onnes [30]. Over the years, superconductivity has been more understood with advanced knowledge and experience in materials and design processes. Then, almost a century later, the SNSPD was demonstrated by Goltsman et al. using the NbN strip (200-nanometer (nm) wide and 5-nm thick) in 2001 [31], and consequently, SNSPD systems have been put to use in the field [32]. After that, numerous studies have been effectively carried out and performed in this field with increased knowledge for years [33]. These detectors consist of a meandering nanowire obtained from a thin layer of superconducting material using nanofabrication techniques. Superconductivity is disrupted locally when a single photon is absorbed in that meandering nanowire. As a result, the current flows toward the circuitry, producing a voltage pulse. Superconductivity in the meandering nanowire quickly recovers once the photon is absorbed, and the SNSPD is ready to detect the next photon [34]. In addition to these detectors, highly promising photon-counting technology for infrared wavelengths [29], recently, SNSPDs have also been developed highly efficiently for the VIS region [35]. Although conventional Si APDs have excellent VIS region efficiency, they exhibit afterpulsing effects after a photon detection event, and therefore, SNSPDs have an essential advantage for more reliable measurements [36]. However, operational requirements can be an economic burden as low temperatures require high cryocooling costs [33]. However, there is no doubt that SNSPDs will have an essential place in many scientific research and practice in the next decade as they do today.

1.2 Key Parameters for SPD Characterization

Photodetector technology is relatively advanced now; however, it has not been developed suddenly, just like other technologies. Over the years, significant effort has been devoted to improving traditional photon-counting detectors and transferring new device concepts into existing technologies for optical quantum information applications. Today, many SPDs are commercially available from a variety of companies. This variety among companies creates competition, and each year, detectors with improved characteristics are launched to the market by pushing the limits of technology.

The performance of SPDs is evaluated in some terms, such as dead time, dark-count rate, timing jitter, spectral range, and detection efficiency. These are significant general benchmarks for the analysis and comparison of SPDs. To accurately characterize the performance of single photon detectors according to these parameters, correct measurement methodologies must be applied [27]. The following parameters are essential to characterize SPDs:

1.2.1 Dead Time

Following the detection of a single photon, a crucial interval ensues during which the detector undergoes a process of restoration and readies itself for the potential detection of another photon. This term is commonly referred to as the recovery time and is tied to both the specific type of detector employed and the intricacies of its associated counting electronics [37]. It is imperative to acknowledge that the duration of this recovery time is not a universal constant but rather exhibits variability contingent upon the inherent characteristics of the detector technology in use. One notable aspect influencing the recovery time is the intentional augmentation of dead time, a deliberate delay implemented in SPDs. This deliberate prolongation of dead time serves a crucial purpose; it mitigates the likelihood of spontaneous retriggering events transpiring within the detector following an initial detection occurrence. By

strategically elongating the dead time, SPDs effectively create a buffer interval that minimizes the potential interference of subsequent events, enhancing the reliability and accuracy of the detection process. Furthermore, it is essential to recognize that the maximum count rate of the detector, representing the number of photons reaching the detector per unit of time (typically measured in seconds), is intricately linked to the dead time phenomenon [38]. The imposition of dead time acts as a limiting factor on the maximum count rate of the detector, thereby establishing a critical parameter that shapes the overall performance capabilities of SPDs.

1.2.2 Dark-Count Rate

Dark counts are false counts recorded by photonic detectors in the absence of light. It is also called dark noise or dark current, which can be caused by the detector's material properties, sensitivity to noise, or biasing conditions [27]. This term is used when the detector gives output as if they were real photon events. For example, electrons and triggering avalanches can be excited by thermal energy. Because of that reason, SPDs generally have cooling units to keep the temperature at a certain level. For example, standard APDs are cooled with compact Peltier cooling in general. These detectors must be contacted with heat-conductive material to dissipate the heat through a heat sink [39]. In addition, the dark count rate is also highly affected by biasing conditions. A difference between the bias and breakdown, which is also known as overvoltage, can lead to a higher dark count rate. Higher overvoltage contributes to the afterpulsing effect, and this is also known as dark pulses. Afterpulsing occurs when the charge carriers are released after being trapped in the avalanche zone, creating an avalanche current again and also increasing with the delay of avalanche quenching [40]. The dark count rate can be measured by blocking the active region of the detector [39].

1.2.3 Timing Jitter (Timing Resolution)

This term refers to differentiation in the time interval between detector photon absorption and the output electrical pulse [27]. Timing jitter is a parameter to consider in many applications where precise timing of photon arrival is essential, such as time-resolved spectroscopy [41], light detection and ranging (LIDAR) [42], or quantum communication [43]. The jitter at half-voltage is usually of the same order of magnitude as the rise time. Because of that reason, the minimum threshold of the rising pulse should be utilized for timing applications when little jitter is required. Timing jitter can be measured by taking the FWHM (full-width half maximum) average of variation in the time histogram [44]. Figure 4 shows a sample setup proposed by Hadfield to measure the timing jitter of a single photon detector. In this setup, a picosecond pulsed laser and high-resolution timing electronics were used to measure the dominant jitter of the detector. The SPD triggers the "start," and the delayed pulse triggers the "stop" for the timing electronics. After accumulating over multiple clock cycles, the histogram of the interval time for the start-stop gives the timing jitter of the SPD.

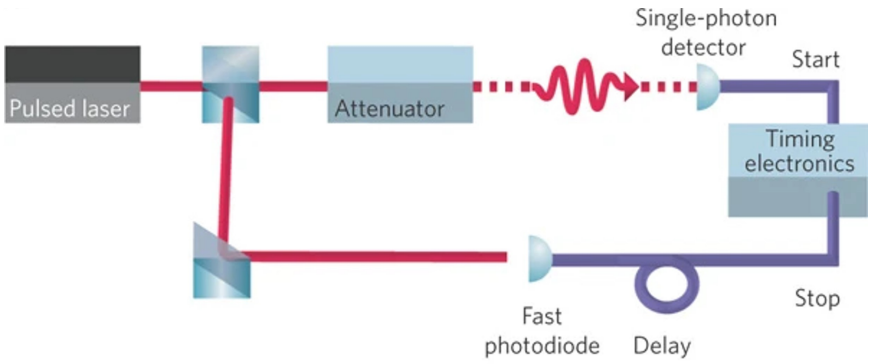

Figure 4: Timing jitter measurement setup [27].

1.2.4 Spectral Range

SPDs are only sensitive to a specific wavelength range that depends on constituent materials [27]. Depending on the desired application, they can be selected at a suitable wavelength range. This intrinsic property, closely linked to materials science, confers a versatile adaptability to SPDs based on the intended application. The selection of materials determines the wavelength range to which these detectors respond, thereby enabling tailored utilization in diverse scenarios. For instance, Si-based APDs are well-suited for applications in the VIS range, offering heightened efficiency in capturing photons within this spectrum. In contrast, APDs leveraging Indium Gallium Arsenide (InGaAs) technology extend their sensitivity into the near-infrared spectrum, providing an advantageous capability for low-light detection at high speeds. This flexibility in wavelength sensitivity allows researchers and engineers to precisely match SPDs with the specific requirements of a given application. For free-space communication applications, there is much interest in commercially available detectors that work at communication wavelengths, as the wavelength of 1550 nm has the lowest optical fiber losses. This strategic alignment of SPD capabilities with the unique demands of optical communication wavelengths positions them as instrumental tools for advancing technologies such as quantum key distribution (QKD), underscoring their significance in the ever-evolving landscape of quantum information and communication [45].

1.2.5 Detection Efficiency

In the comprehensive assessment of detector performance, detection efficiency stands out as a pivotal parameter, offering insights into the efficacy of these devices. This metric, fundamentally defined as the probability that a photon striking the detector will be successfully registered, serves as a critical gauge of the responsiveness of the detector to incident photons. The ratio of the detected number of counts to the predicted

number of counts arrives at the detector that is assumed to work at full efficiency. A notable factor influencing detection efficiency is the temperature at which the detector operates. As elucidated by research [46], lower temperatures generally yield higher detection efficiency. The rationale behind this correlation lies in the relationship between temperature and dark counts. Dark counts, indicative of spurious signals in the absence of incident photons, tend to increase with rising temperatures, consequently diminishing the overall detection efficiency. Therefore, the strategic control of temperature emerges as a crucial parameter for optimizing detection performance. Moreover, the wavelength of incident photons is linked to quantum efficiency, which is the efficiency of a detector in converting incident photons into detectable signals [47]. Because each detector has its own particular spectral range depending on its material composition and exhibits a unique spectral range, they have more quantum efficiency at specific intervals. This wavelength-dependent quantum efficiency further underscores the importance of tailoring detectors to specific spectral requirements, ensuring optimal performance within designated wavelength intervals. In essence, the interplay between temperature, dark counts, and wavelength-dependent quantum efficiency shapes the overall detection efficiency, delineating the nuanced factors governing the operational prowess of these detectors across diverse applications and environmental conditions.

1.3 Commercially Available SPDs

In this section, some SPD technologies were examined in terms of their present performance and potential for the future. As mentioned before, there are many SPDs commercially available in the market. These detectors, together with their electronics, can be used for single photon measurement in many applications. The commercial availability of numerous SPDs from different brands offers a spectrum of choices, allowing for tailored solutions in diverse fields. The efficiency, spectral range, dark

count, count rate, and other performance metrics exhibit a wide range within this array of detectors. This diversity not only accommodates the unique requirements of various scientific and technological domains but also paves the way for continuous innovation and refinement. As technology advances, the evolving landscape of SPDs anticipates an exciting future where enhancements in sensitivity, temporal resolution, and quantum efficiency are poised to revolutionize photon detection capabilities. The integration of SPDs with cutting-edge electronics is expected to unlock new possibilities, fostering breakthroughs in fields ranging from quantum communication to biomedical imaging. In essence, this exploration of SPD technologies transcends the present, offering a glimpse into a future where precision and versatility in single photon measurements become indispensable tools across scientific and industrial frontiers.

The PMT is the most well-known and enduring photon-counting technology to the present. Commercial PMT units are widely accessible, and there are ongoing efforts to improve these devices. This technology may be produced by hand and customized to the specifications of the customer [48]. Since their properties, such as shape, spectral response range, and wavelength range, can be changed, PMTs have been utilized in different fields with a wide detection wavelength range. There are many commercially available PMTs in the market with different performance variations. Their photocathode active area diameter size can be as low as 5 mm [49], and they cover the spectral range of 115 to 1700 nm [50]. With GaAsP photocathodes, PMTs have a maximum efficiency of about 40% and dark count rates down to 100 Hz [27]. The PMT module offered by Hamamatsu, shown in Figure 5 [51], exemplifies the current state of technology by providing a glimpse into the dimensions of PMTs of today.

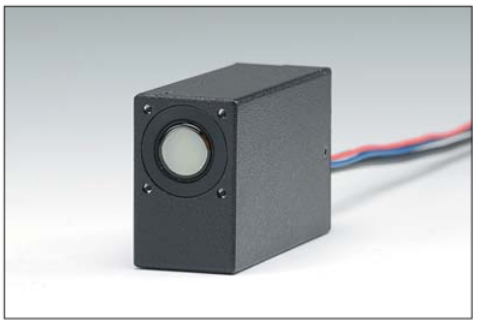

Figure 5: A photo of the PMT module offered by Hamamatsu [51].

Many SPDs based on APD technology provide an alternative to PMTs in laboratory quantum optics experiments and free-space QKD systems. APDs, together with their driver circuits, can be used for single photon counting applications with high detection efficiencies, low dark count rates, and high count rates in the VIS to near-infrared range. The user can design these driver circuits or purchase from different brands that offer their module form. There are new generations of SPADs in the market. These devices offer low operating voltages, low dark count, low afterpulsing probability, and low timing jitter. In general, their active areas range from micrometer (µm) to millimeter (mm) units, and the operating voltage is low at around 150 V [52]. There is a SPAD module offered commercially that has a typical 7 cycle per second (cps) extremely low dark current with a spectral response range of 370 to 900 nm and achieves a typical 45% photon detection efficiency [53]. There is another SPAD module newly released and offered by the same company, with a photosensitive area of 50 µm, a typical 20 cps dark current at the 400 to 1000 nm spectral range, and a peak sensitivity of 630 nm [54]. Another Si SPAD compact module that is commercially available has an active sensing area diameter of 50 µm with a dark count rate that is less than 200 cps. The timing is improved to 50 picoseconds (ps) at FWHM, and the detection efficiency is up to 50% at 400 nm, but it is reduced to 5% at 800 nm [55]. A photo of the product with its control unit is shown in Figure 6.

Figure 6: A photo of FastGated-SPAD offered by MPD [55].

A SPD module based on Si SPAD offered by the different company has a very thin active area diameter of 20 µm with a typical 25 cps dark count rate, 25 MHz maximum count rate, and 35% typical photon detection efficiency at 500 nm [56]. Some commercially available Si SPADs with operating voltage at around 400 V (Volts) provide high sensitivity with a thick sensitive area. These devices also have single-photon sensitivity in the 400 to 1000 nm spectral range. There are many InGaAs-based APD technologies as these detectors can be used in telecommunication wavelengths [27]. They have high-speed response of up to 1.6 GHz and wavelength covering 850 to 2500 nm [57]. They offer high speed, high sensitivity, and low noise [58], but these devices experience orders of magnitude more dark count rates than their Si counterparts as a result of material flaws [27].

As mentioned earlier, SPD technology based on the superconducting nanowire is emerging. Although this technology is still mainly in the research phase and is less widely available commercially than the other mentioned technologies, some companies offer their products based on this technology. ID Quantique Company has offered SNSPD with high detection efficiency, timing precision, low noise, and fast recovery time. Figure 7 shows a photo of this product. This product has a high system detection efficiency across hundreds of nanometers, centered on a user-selected wavelength from 500 nm to 2000 nm. With built-in cryogenic amplifiers, the detector timing jitter is less than 40 ps FWHM and can reach less than 25 ps. The dark count rate of the detector is also ultra-low, reaching less than 1 Hz [59]. These detectors are

a significant competitor for SPADs replacing PMTs. The long wavelength sensitivity of the SNSPDs is much better than Si SPADs, and the SNSPDs have a higher signal-to-noise ratio than the InGaAs SPADs [29].

Figure 7: A photo of SNSPD offered by ID Quantique Company [59].

1.4 SPDs in Defense and Industry

Quantum cryptography, which is one of the areas where SPDs are used, is of great importance for the defense field. Attacks on the security networks protected by strong algorithms will pose a serious threat when a quantum computer becomes available. Because of the probabilistic nature of quantum mechanics, a quantum-based communication system shows resistance against this danger to ensure secure communication [60]. The main goal of these applications is to provide secure communication by detecting the keys distributed by the source in entangled-based systems by two target users. In such a system, the measurement of entangled photons is carried out by using these detectors [61]. In Figure 8, an example optical scheme of the QKD proposed by Anton Pljonkin et al. is shown. They reported that a QKD system (QKDS) does not work without initial synchronization, a process during which the key parameters of the detection equipment are established. In this QKDS configuration, synchronization consists of the measurements of the path length and propagation path of the optical emission between the transceiver and encoding stations. SPADs operating in

single-photon counting mode play a crucial role in registering the attenuated optical emission in both directions in the same fiber-optic line, and this synchronization is based on detecting optical pulses by photodetectors. It is known that a strong optical signal sent over a communication channel can be at risk of unauthorized access, as someone might divert part of the light. To address this issue, they proposed developing synchronization algorithms to enhance the security of QKDS. A unique characteristic of this algorithm lies in its utilization of attenuated optical pulses as signals for synchronization [62].

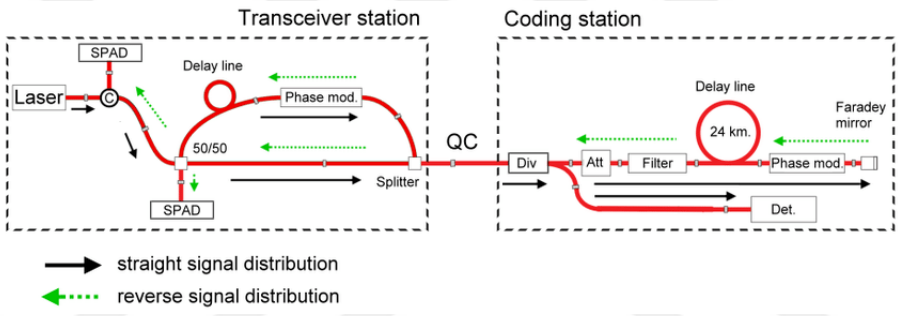

Figure 8: An example optical scheme of the QKD [62].

SPDs are also used in the LIDAR system for various applications areas such as the automotive [63] and defense. Vision systems, which can obtain both two-dimensional and three-dimensional information with LIDAR, are gaining increasing importance, especially with automotive companies that tend to develop self-driving vehicles. These detectors are expected to have high quantum efficiency and fast counting with accuracy in such applications where precision is crucial. Single photon detection, with its quantum limit sensitivity, plays a crucial role in advancing various fields of modern physics, biology, chemistry, and astronomy. In the field of quantum information, single photon sources are integral components, and SPDs are essential for characterizing these sources. They offer valuable insights into features like spontaneous emission lifetime, $g^2(\tau)$ measurements [64], and photon statistics of the source [65]. The ideal detector for these applications should exhibit zero dark counts, high-speed operation,

and high quantum efficiency at the desired wavelength. These characteristics are essential for obtaining accurate and reliable data in quantum information research. Additionally, different detector technologies find widespread use in diverse techniques that allow non-destructive examination of the physical and chemical structure of materials based on their interaction with light [66]. Figure 9 shows an example optical layout for fluorescence lifetime spectroscopy measurement using a SPAD array detector. In this layout, a 375 nm picosecond diode laser is used to generate the excitation light. A specially designed fiber bundle is employed to handle both delivering the excitation light and collecting the resulting fluorescence signal. The excitation fiber is marked in blue, while the green-highlighted fibers, numbered for identification, are responsible for collecting the signal. At the detection end, the thirty-two collection fibers are arranged vertically, with the fiber closest to the excitation placed at the top. This detection configuration ensures that fibers closest to the excitation, providing information from the surface layers, are imaged at the top rows of the SPAD array. Fibers situated farther from the excitation, offering insights into deeper layers, are imaged at the bottom rows of the detector. After that, a representative intensity map of the SPAD array encoding spectral and depth information is obtained [67].

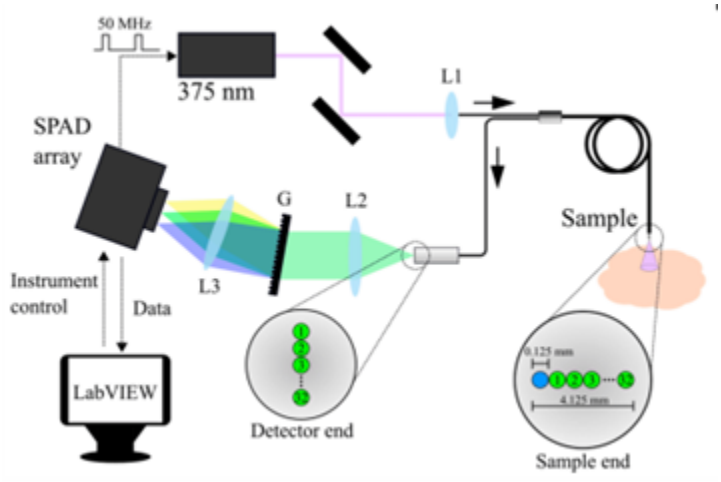

Figure 9: An optical layout for fluorescence lifetime spectroscopy [67].

SPDs are also utilized in medical applications, particularly nuclear medicine, radiation therapy, and imaging technology [68]. Detection of high-sensitivity radiation is essential for the diagnosis and treatment process [69]. In the last 20 years, single-photon emission computed tomography (SPECT) has gained wide interest for clinical applications. The combination of computed tomography and SPECT in a single imaging system provides anatomical localization to differentiate physiological uptake from related disease, as well as patient-specific attenuation correction to increase the visual clarity and quantitative accuracy of the SPECT image [70]. The improvements in features that determine the detector's performance, such as detection efficiency and spatial resolution, will contribute to this field for more accurate diagnoses. The usage of SPDs is also well-suited for other imaging applications such as fluorescence lifetime imaging [71], machine vision, and 3D imaging [72] with extremely high temporal resolution. An example experimental setup using SNSPDs for imaging applications is shown in Figure 10. In this experiment, a light source is employed to illuminate an object, and this illumination is then directed onto a digital micromirror device (DMD) under the control of a digital light processor (DLP). Then, the DMD probes the object using matrices derived from randomly selected rows of columns that have been permuted randomly in a Hadamard matrix. The projection of the object onto the DMD sampling matrix results in a unique total intensity reflected off the DMD for each specific sampling matrix. Subsequently, employing another set of imaging optics, the reflected pattern is projected onto an 8x8 SNSPD array housed within an optical cryostat, which is cooled to approximately 1 Kelvin. Given that the light is coupled onto the SNSPD array through free space, a series of optical filters located within the cryostat serves to eliminate any black body radiation originating from the room temperature environment [73].

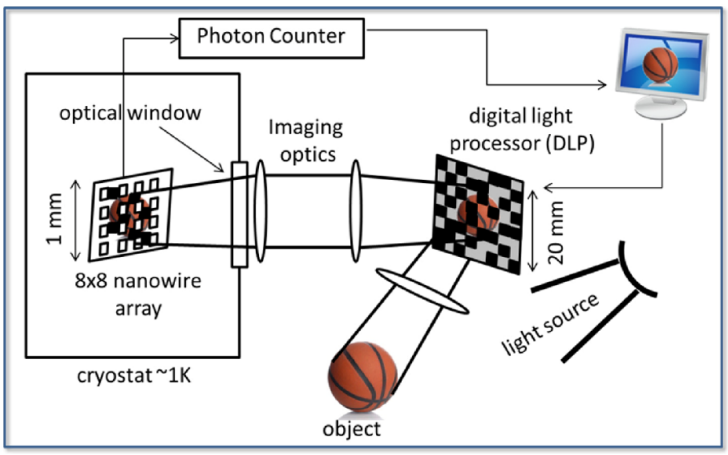

Figure 10: An example experimental setup for imaging applications [73].

SPDs are up-and-coming technologies in the field of quantum information and communication, which are ever-evolving in our modern society with the increase of online communication. Some studies are working on underwater optical wireless communication (QWC) based on single photon detection. SPDs are used to achieve long-distance communication by detecting very weak light signals, and the transmission range of a QWC system can be efficiently increased by using an SPD as a receiver. They are also used in different areas, such as land and space, which are especially critical for the transmission of secure messages [11]. SPD technology opens a new path for space research and applications. Development in the solid-state SPDs allows for testing deep-space optical communications, single-photon laser ranging, and fundamental laws of physics in space. However, SPD's noise performance, reliability, and durability are constrained by the harsh conditions in space, such as the increased radiation flux and thermal vacuum. Mitigating these effects is vital to enabling new space applications that require high-fidelity single-photon detection. There is a lot of research interest in special shielding structures, cooling technologies, and configurable electronics to increase reliability [74, 75]. Since the early 2000s, the widespread adoption of single photon detectors, especially SNSPDs, has revolutionized several technological fields. These detectors play a crucial role in cariogenic technologies,

especially in the field of quantum information applications. The ability of SNSPDs to detect coincidences between entangled photons is very important to the success of many experiments in quantum information science. As technology continues to advance, the complexity of experimental setups increases, forcing researchers to push the boundaries of what is possible. Notably, the applications of SNSPDs extend beyond the realm of quantum information. They present a versatile solution for sensing applications, offering a viable alternative to traditional InGaAs SPADs [29]. These detectors are attracting interest in various fields, with important application areas such as QKD [61], communications [76], quantum computing [77], depth ranging [78], sensing [79, 80], and integrated circuit testing [81]. The versatility of SNSPDs positions them as indispensable tools for advancing technology in a variety of fields, demonstrating their potential impact on a wide range of scientific and technological endeavors.

CHAPTER II

THE AVALANCHE PHOTODIODE

As an advanced form of the conventional photodiode, the APD plays a crucial role in numerous applications, offering enhanced sensitivity and signal amplification capabilities. Understanding the fundamental aspects of both the photodiode and its avalanche counterpart is essential for grasping their applications in diverse fields such as telecommunications, LIDAR, and medical imaging. This chapter unfolds in two sections: "Photodiode Structure and Working Principle" and "APD Structure and Working Principle." Before delving into the detailed exploration of the structure and working principle of APD, it is important to gain a comprehensive understanding of the overarching characteristics and significance of the photodiode.

2.1 Photodiode Structure and Working Mechanism

A photodiode, a light-sensitive semiconductor device, generates electric current when it absorbs photons. Semiconductor materials such as Si, Germanium (Ge), and Indium Gallium Arsenide (InGaAs) used in a photodiode determine the properties of the diode, such as its sensitivity to wavelengths in the spectrum. The photodiode has a p-n junction or PIN structure [82]. The term "PIN" in photodiodes refers to a specific structure that involves three main layers: the p-type semiconductor layer, the i-type (intrinsic or undoped) layer, and the n-type semiconductor layer. The intrinsic layer is sandwiched between the p-type and n-type layers. The primary purpose of the intrinsic layer is to reduce the capacitance of the device, allowing for faster response times and improved sensitivity. The PIN structure is commonly employed in photodiodes for applications requiring high-speed response and enhanced performance. On the other hand, the p-n junction is a more traditional structure featuring two

main layers: the p-type and n-type semiconductors directly adjacent to each other. This configuration forms a junction where electrons from the n-type layer and holes from the p-type layer combine, creating an electric field. When photons strike the photodiode, they generate electron-hole pairs at the junction, leading to a flow of electrical current. These junction photodiodes are widely used and offer simplicity in design. However, they may have higher capacitance compared to PIN photodiodes [83]. Figure 11 illustrates an example of a p-n junction structure formed by doping semiconductor materials and bringing them into contact.

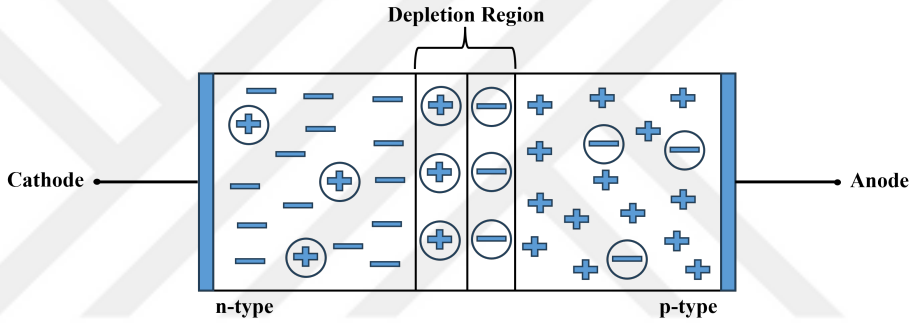

Figure 11: Illustration of p-n junction.

Doping, a process to increase charge carriers, results in a p-type region with excess holes and an n-type region with excess free electrons. The holes and electrons in the p-type region are called majority and minority carriers, respectively. Similarly, the electrons and holes in the n-type region are called majority and minority carriers, respectively. Because of the concentration difference, the majority of electrons and holes diffuse in other regions when both areas are in contact, and this diffusion causes a depletion region at the junction. At the same time, there is an electric field from positive charges in the n-type region to negative charges in the p-type region. This potential difference limits the diffusion amount and determines the thickness of the depletion region [84].

The structure of photodiodes forms the basis for understanding their operational principles. These devices consist of a p-n junction, a light-sensitive region exposed

to incident photons, and metal contacts for collecting charge carriers. Within this structure, the key working mechanism begins to unfold when photons strike the light-sensitive region. When photons strike the light-sensitive region, they are absorbed by the semiconductor material, creating electron-hole pairs. The electric field at the p-n junction causes the photo-generated electrons to drift toward the n-side and the holes to drift toward the p-side. As electrons and holes reach the respective contacts, they generate an electrical current, which is proportional to the intensity of incident light. There are several types of photodiodes, including PN photodiodes, APDs, Schottky photodiodes, and PIN photodiodes. They all serve as the foundation for numerous light detection and sensing technologies across various industries. Their simple yet effective structure and working mechanism make them indispensable in applications ranging from everyday light detection to advanced optical systems [85].

2.2 Avalanche Photodiode Structure and Working Mechanism

APDs are a type of photodetector that can convert light into electricity and have a similar structure to a PIN junction. They are essential parts of systems in applications requiring high sensitivity, low noise, and high-speed photon detection. Known for their remarkable sensitivity, low noise characteristics, and high-speed photon-detecting ability, APDs have become essential parts of many cutting-edge applications. These applications are very diverse, spanning from telecommunications and medical imaging to remote sensing and quantum communication. The robust structure and reliable operation of APDs make them indispensable for harnessing the potential of light detection and photon counting across diverse fields.

The core of the distinctive structural design of APDs is its high-field avalanche region, and this critical region features a strong electric field, much more potent than regular photodiodes. This electric field is essential in accelerating photo-generated charge carriers and causing impact ionization, leading to avalanche multiplication.

The avalanche multiplication process begins at the avalanche zone boundary, which is located directly adjacent to the high-field region. Here, the strong electric field provides carriers with the energy they need to generate additional electron-hole pairs through impact ionization. The APD also retains a conventional p-n junction, separating the carriers generated by photon absorption and guiding them toward the high-field region. Material selection is crucial, with high-purity semiconductor materials such as silicon or III-V compounds like InGaAs commonly used due to their high absorption coefficient in the desired wavelength range. Additionally, metal contacts on the p-type and n-type regions are essential for collecting avalanche-generated charge carriers and facilitating electrical current flow. A protective enclosure is often utilized to enhance light detection and ensure the safety of the APD. This enclosure may include lenses or optical elements to amplify sensitivity. These structural elements combine to enable avalanche multiplication in the APD, resulting in a significant gain in output current compared to conventional photodiodes [86].

The working mechanism of APDs constitutes a critical aspect of their design. The operation of APDs built on a structural foundation is first initiated by exposing the photosensitive region to incoming photons. Photons hitting the light-sensitive region are absorbed by the semiconductor material, resulting in the generation of electron-hole pairs. What distinguishes APDs is their application of high reverse bias voltage, commonly referred to as the breakdown voltage. A single electron-hole pair generation can start a self-sustaining avalanche current in the milliampere range at such bias because the electric field in the depletion layer is so strong. The current keeps flowing until the avalanche is quenched by lowering the bias voltage below the breakdown voltage; the SPAD must then be reset to the quiescent bias level in order to detect subsequent photons, making APDs fundamental components in high-sensitivity photon detection applications [87]. Figure 12 illustrates the avalanche operation process of a SPAD in Geiger mode. A photon that strikes the photodiode

causes the generation of electron-hole pairs to dramatically increase in the high electric field in the multiplication area.

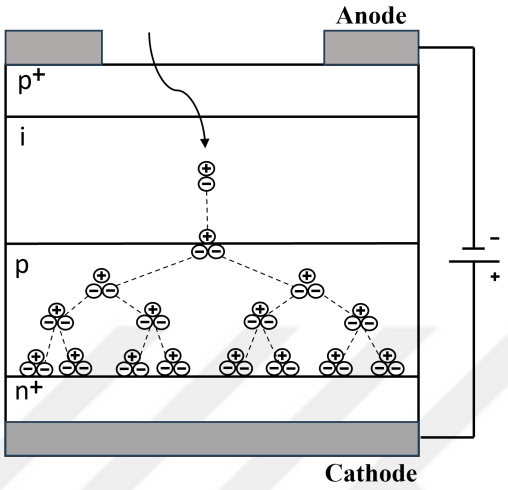

Figure 12: SPAD working principle.

2.3 The Selected Photodetector Information

In this study, the focus was on utilizing the TO-8 SAP500 series Si APD provided by Laser Component for single photon detection. The SAP500 series features a unique "reach-through" construction designed to offer high gain, exceptionally low noise levels, and elevated quantum efficiency, particularly suitable for applications with very low light levels. This APD may be used in linear mode with a gain of up to 250 or greater if the bias voltage is less than the breakdown voltage or in the "Geiger" mode to enable the detection of single photons if the bias voltage is higher than the breakdown voltage. Its adaptability makes it applicable in a wide range of challenging scenarios, from LIDAR systems to the sensitive detection of small fluorescence signals.

The selected photodiode package is fiber-pigtailed and incorporates two thermoelectric cooler (TEC) sections designed to minimize thermal noise, which is particularly beneficial for detecting extremely low signals. This feature allows the diode to operate at a temperature as low as -18 °C while maintaining a temperature of 22 °C.

At this temperature, the APD exhibits a high photon detection efficiency and low dark count rates. Maintaining a constant temperature for the APD is crucial due to the temperature-dependent behavior of the breakdown voltage. The reason for this is that the breakdown voltage increases with the temperature increase, and the detection efficiency decreases accordingly. Conversely, as the temperature decreases, the breakdown voltage decreases, and accordingly, the increase in voltage drop on the APD causes the detector to perform a dark count as a result of increasing the electric field across the junction and raises the rate of avalanche [46]. To address temperature fluctuations, a TEC is a reliable solution, enabling consistent voltage and performance across a broad temperature range. The integrated thermistor in the package was used to monitor the APD temperature and make the TEC feedback loop circuit. A suitable heat sink was employed to dissipate the heat generated by the detector. Figure 13 shows the thermistor curve of the photodetector, illustrating its response to temperature changes [88]. In essence, the TO-8 SAP500 series Si APD, with its specialized construction and integrated TEC system, emerges as an adaptable solution for single photon detection, ensuring reliable performance across varied environmental conditions. This research leverages the capabilities of this photodiode to advance applications in fields such as LIDAR and fluorescence detection.

The TO-8 package SAP500 series Si APD is designed for optimal performance in the wavelength range of 400 to 1000 nm, featuring a 500 um diameter active area and a peak sensitivity at 700 nm. Its detection efficiency is up to 65% at 830 nm, and the dark count rate is a typical 2000 counts per second (cps). At 22 °C and a photon detection probability of 5% for 830 nm, the voltage above the breakdown voltage is 2V. Additionally, the afterpulsing ratio, an indicator of the likelihood of subsequent pulses occurring after the initial detection, is 2% under the specified conditions [44]. These specifications, provided by Laser Components, position the SAP500 series Si APD as a high-performing and versatile photodetector suitable for a range of applications,

from scientific research to telecommunications, where precision and sensitivity are paramount.

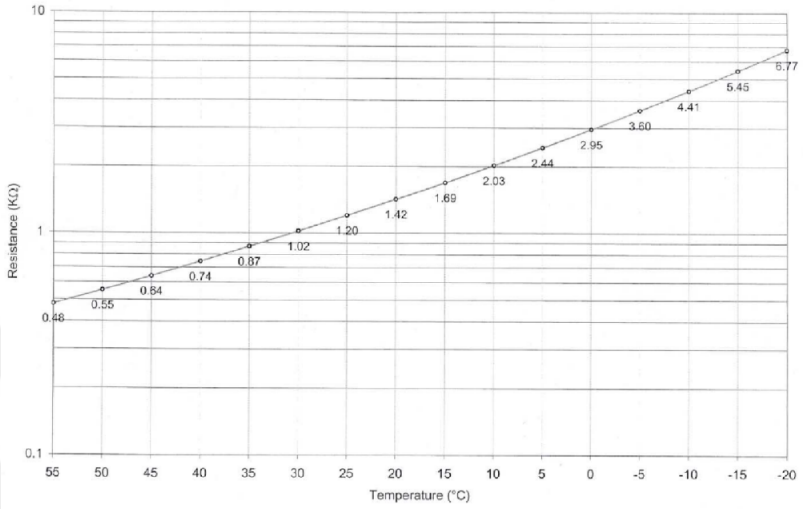

Figure 13: TO-8 SAP500 series Si APD thermistor curve [88].

CHAPTER III

EXPERIMENTAL PART

The experimental part dedicated to SPD emerges as a crucial chapter, connecting theoretical frameworks with the practical complexities of detecting and analyzing single photons. This critical juncture signifies a shift from abstract concepts to hands-on exploration, where the overarching objective is to validate and extend our theoretical understanding. Technological integration, incorporating cutting-edge advancements in photodetector technologies, provides a useful addition to our setups.

At the core of the experimental setup is the use of the SPAD, which exhibits its unique ability to initiate an avalanche current when a photon hits it in the reverse bias beyond breakdown voltage (V_{BR}). This avalanche current occurs with exponentially increasing electron multiplication within picoseconds and continues if it is not quenched. Quenching occurs when the voltage applied to the SPAD falls below the V_{BR}, and during this process, the SPAD is not able to detect a photon. Finally, the SPAD is restored to the sensing condition, and the process repeats itself for each event [89]. Avalanche quenching is operated in two ways: passive quenching (PQ) and active quenching (AQ). PQ circuits use passive circuit elements and are very useful for SPAD device testing and selection [90]. Figure 14 illustrates a sample schematic of a basic passive quenching circuit. The SPAD is connected in series with a relatively large ballast resistor for passive quenching, and when a photon is detected, the voltage drop across the resistance quenches the breakdown. The dead time that results from the time it takes to recharge its junction capacitance (C_J) using the ballast resistor gives the SPAD a chance to recover from the detection [40].

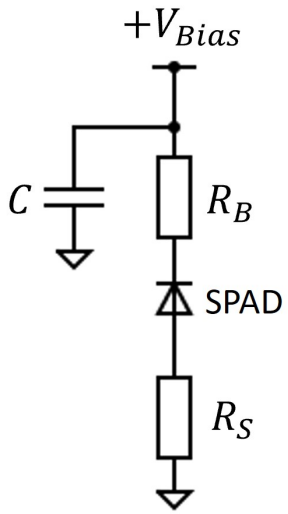

Figure 14: A sample schematic of the PQC.

In the AQ circuits, the voltage provided to the SPAD is changed by active electronics components [89]. A sample schematic of AQC is given in Figure 15. Properly designed AQC makes it possible to take advantage of the best performance of the SPAD [90]. In this case, the existence of a photodetection is detected after the event, and the voltage provided to the SPAD is changed to below the breakdown voltage by surrounding electronics (quenching switch) as soon as possible. This leads to a fast recovery and well-defined dead time. Finally, the SPAD is set to the sensing condition, and the process repeats itself for each event [90]. In the figure, V_{ex} (it can also be called overvoltage) refers to the difference between bias (V_{Bias}) and $V_{BR}(V_{break})$, and it is given as:

$$V_{ex} = V_{Bias} - V_{BR}$$

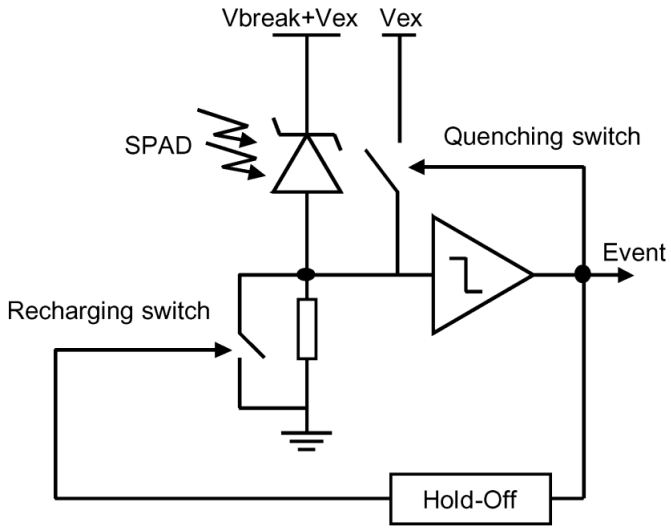

Figure 15: A sample schematic of AQC [89].

3.1 Quenching and Temperature Control Circuit Topologies

In this study, the PQ circuit with temperature controller by using the TO-8 SAP500 series Silicon APD was designed for single photon detection in the VIS range. The schematic of the PQ circuit is shown in Figure 16. The SPAD D1 is connected in series with a relatively large ballast resistor, R1. When a photon is detected, the voltage drop across the resistance quenches the V_{BR}, and the dead time gives the SPAD a chance to recover from the detection. The voltage of the capacitor C3 output that is used to measure high-frequency avalanches is compared with the constant reference voltage by the comparator U2. Then, D flip-flop U1 outputs high when the comparator output is high, which is the "there is a photon" case, and outputs low when the comparator output is low, which is the "there is no photon" case.

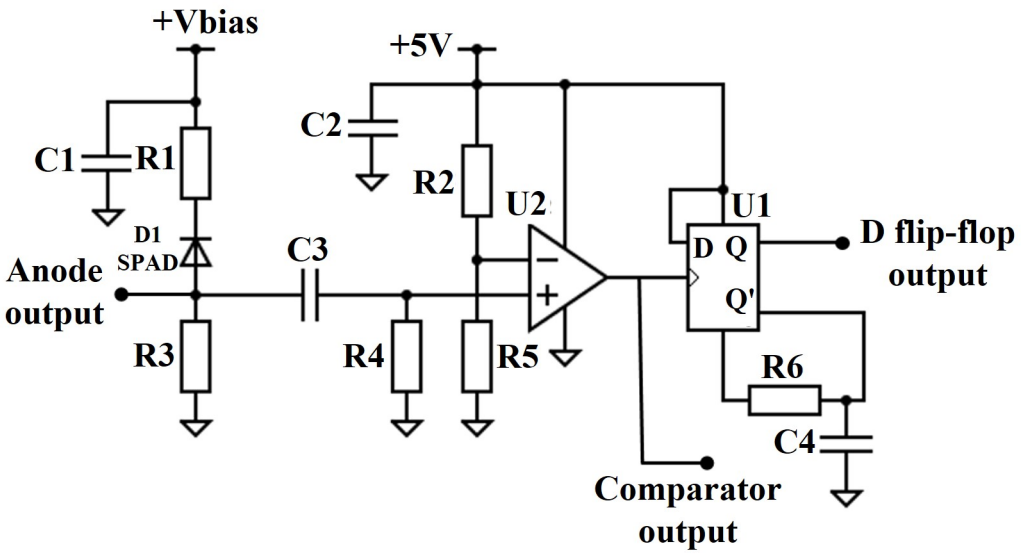

Figure 16: The schematic of the single photon detection circuit.

As mentioned earlier, V_{ex} is very important for the performance of the detector. When the temperature of the SPAD varies, it is necessary to change the operating voltage or reduce the temperature of the SPAD to maintain the same gain while maintaining the same V_{ex}. If the temperature of the SPAD decreases, its breakdown voltage decreases, and its gain increases at a constant bias voltage and wavelength. Therefore, cooling the detector is advised to increase the detected photocurrent. On the other hand, the dark current increases when the temperature decreases. At a temperature of 0 Kelvin (K), the maximum dark current is obtained, which is equal to the saturation current [91]. Therefore, it is essential to find an optimal condition by not using a very small overvoltage that will lead to little gain or a very high overvoltage that will lead to high dark counts.

To maintain the same V_{ex}, TEC operation was used to keep the temperature of the SPAD at the same level. The Peltier effect, which is the transmission of heat when current passes through a conductor, is the basis of the TEC process. The schematic of the temperature controller is shown in Figure 17. The temperature of the SPAD is sensed by the thermistor (THR), which is located very close to the SPAD in the same

package. According to the detected temperature, a signal is sent to the TEC pins of the SPAD using the feedback circuit. The THR in the SPAD package is connected to R10 and R13 for APD temperature feedback. R10 is supplied by the 3.3 V zener diode D2 by the current-limiting resistor R9. The remaining parts consist of three equal-values of 6.8 kΩ resistors: R10, R12, and R13. These resistors control the temperature of the detector and determine the reference value for the error, which is the difference between the voltages R12 and R13 detected by the U3 LM358. The operating temperature of the APD is monitored using the OUT2 voltage. The OUT1 voltage is connected to a trimpot VR1 to adjust the TEC current by controlling the emitter current of transistor Q1 [91]. A suitable heat sink was used to dissipate the heat generated by the SPAD.

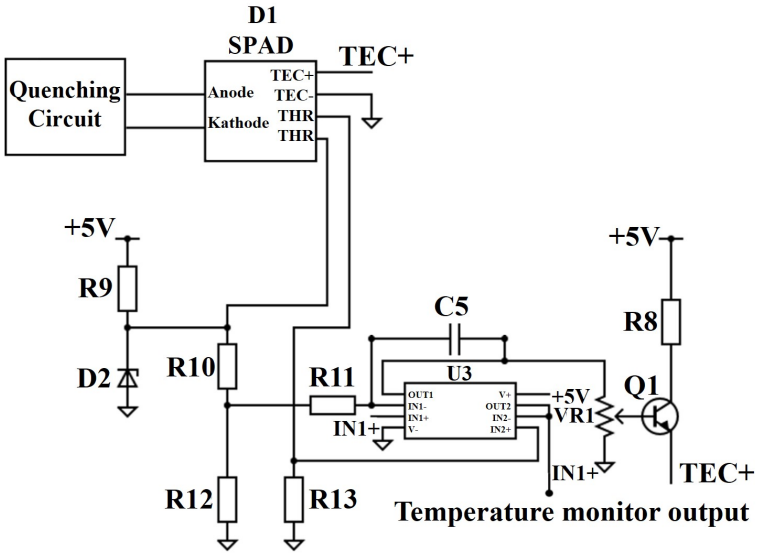

Figure 17: The schematic of the temperature controller circuit.

3.2 Power Supply Circuit Topology

A combination of high voltage for bias and a 5V DC power supply is used in the quenching and temperature control circuit board. The schematic of the power supply is shown in Figure 18. The strategic use of these power sources is very important

for the effective functioning of the circuit. Maintaining a clean DC output is critical to minimizing electronic noise on the final outputs. Great care has been taken in selecting components and designing circuits to achieve this goal. This dual focus on component quality and thoughtful design underlines the commitment to achieving optimal performance and reducing potential interference in the electronic system. The power circuit board can be used by connecting to the grid directly with an adaptor that converts 220V AC to 5V DC. The adaptor output is connected to both a 5V regulator, U1, which was used to maintain a constant voltage level, and to a 5V DC-12V DC converter, U2. The 5V regulator output as a supply voltage is connected to the circuit where quenching and temperature control are located by twisted-pair cable. 12V DC is connected to the TS Series Matsusada high voltage power supply, and a voltage divider with a trimpot VR1 controls the voltage of the power supply. The TS Series high voltage DC-DC converter is very suitable for biasing the APD with low ripple (less than 10 m$V_{peak-peak}$), low noise, and PCB mountable miniature size.

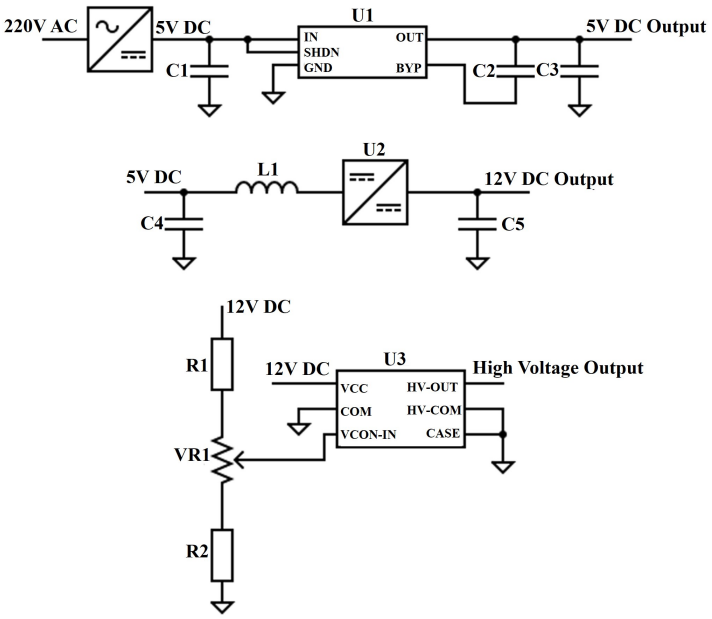

Figure 18: The schematic of the power supply circuit.

3.3 Schematic and PCB Designs

The PQ circuit with temperature controller and the power supply cards were designed in two sections for convenience. When there was a design change in the PQ circuit with temperature control, it was possible to make changes on a smaller circuit without all that design, manufacturing, and assembly process. This provided a more modular approach to problems, and it was cost-efficient. In addition, the risk of thermal noise, which may occur due to the heating of the power supply board, affecting the analog and digital signals on the PQ board, was reduced.

Schematics and PCBs were designed in Altium Designer. The schematics of the PQ with the temperature controller card and the power card are shown in Figure 19 and Figure 20 respectively. The first schematic, as shown in Figure 19, mainly consists of five elements: power connectors, APD, comparator, D flip flop, temperature controller, and output connector parts. On the power input connectors side, the diagram illustrates the bias employed for the APD and the +5V DC supply for other integrated circuits. The quenching mechanism is detailed within the APD section, followed by the digitization of the output analog signal in the comparator-D flip flop segment. All signals to be measured are connected to SMA connector outputs. This comprehensive arrangement ensures the proper functioning of the single photon detection system, where each component plays a crucial role in the overall performance. The schematic design provides a visual representation of the intricate interplay between power supply, photon detection, signal processing, and temperature control, forming the foundation for accurate and reliable measurements in the experimental setup.

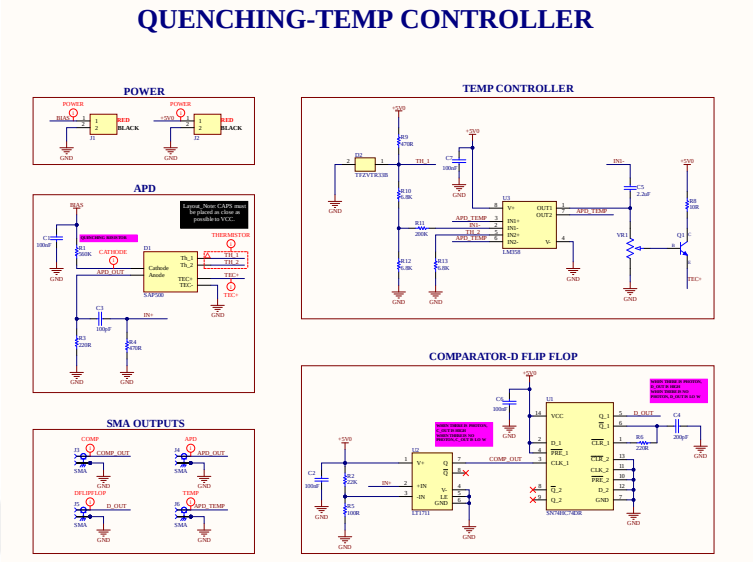

Figure 19: The schematic of the PQ with the temperature controller card.

The second schematic, as shown in Figure 20, mainly consists of four elements, which are V IN - +5V DC, V IN - +12V DC, +12V DC - +High Voltage DC, and output connectors parts. The supply voltages on the quenching with the temperature controller card are provided through the power card. The output power signals are shown in the output connectors section.

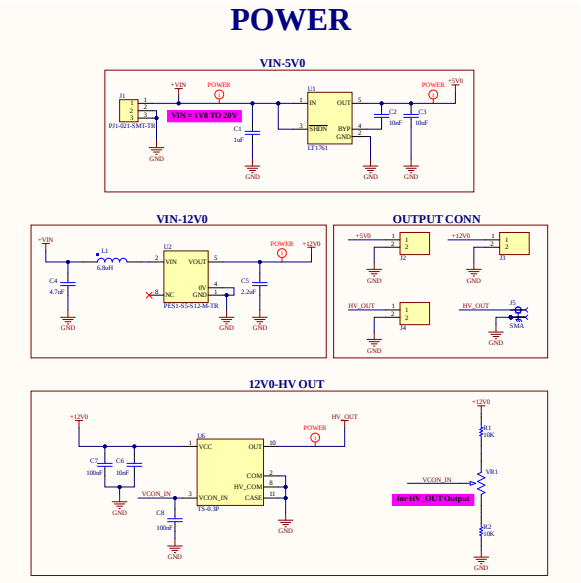

Figure 20: The schematic of the power card.

In Figure 21, the power tree illustrates the power distribution for both the power and quenching with the temperature controller card. The quenching with the temperature controller card has a maximum power consumption of 0.2W, while the power card can provide a maximum of 0.65W. The nearly threefold difference between power values signifies a robust margin, ensuring effective and reliable system operation. This surplus in power availability contributes to the stability and efficiency of the overall system design.

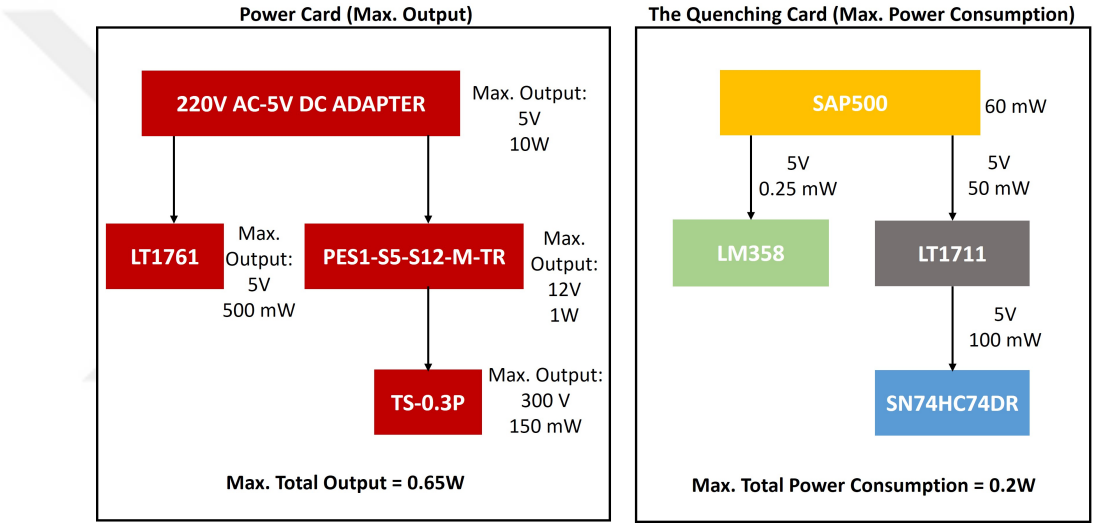

Figure 21: The power tree of the cards.

The PCB drawing is shown in Figure 22, and the mechanical drawing is shown in Figure 23. The size of the quenching and temperature controller circuit board is 90 mm x 109 mm x 1.6 mm, and the size of the power circuit board is 82 mm x 54 mm x 1.6 mm. The diameter and hole size of the vias are 1.6 mm and 0.8mm, respectively. The minimum and maximum width of traces are 0.3 mm and 2.5 mm, respectively. Wider and shorter tracks are used as much as possible for power and signal lines, taking into account impedance matching to have less inductive and capacitive effects. Emphasizing the significance of signal integrity, particularly in PCBs featuring high-speed signals, underscores the critical utilization of a split ground plane. Since digital components in the circuit have a very fast rise and fall time, the adoption of

a solid ground plane is imperative for the quenching and temperature control circuit board. Digital and analog components are assembled far from each other to mitigate the potential for unwanted coupling effects. The preference for surface mount devices (SMD) in most component selections is based on their advantageous attributes, notably their reduced footprint and spatial coverage. A photo of the single photon detection system after the manufacturing and assembly process is shown in Figure 24. An aluminum heat sink was used to dissipate heat from SPAD by enlarging the area, as seen in the figure. The total mass of the system is 90 gr.

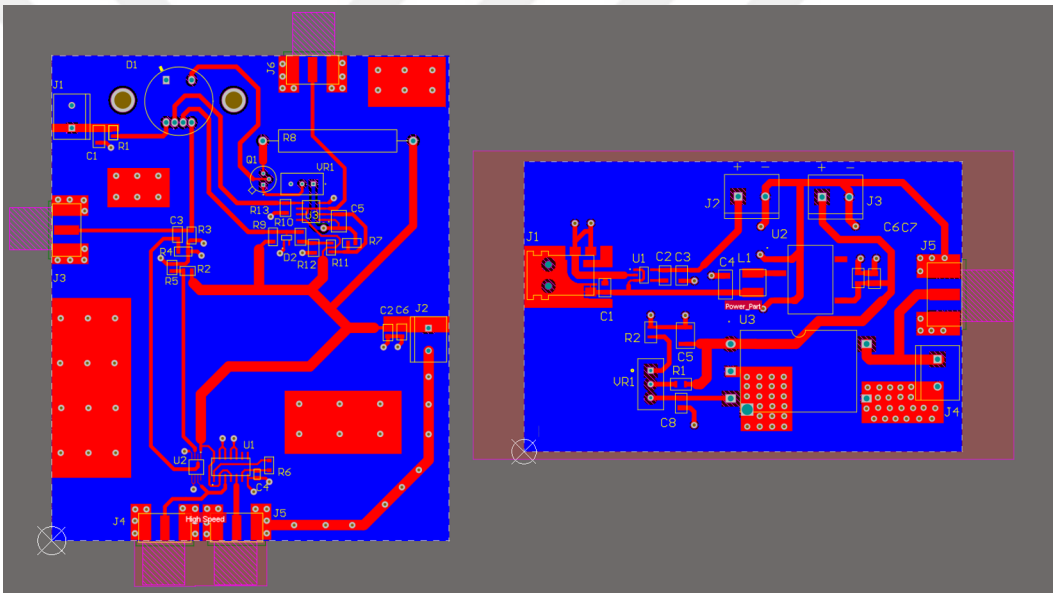

Figure 22: PCB drawing (left: quenching circuit, right: power circuit).

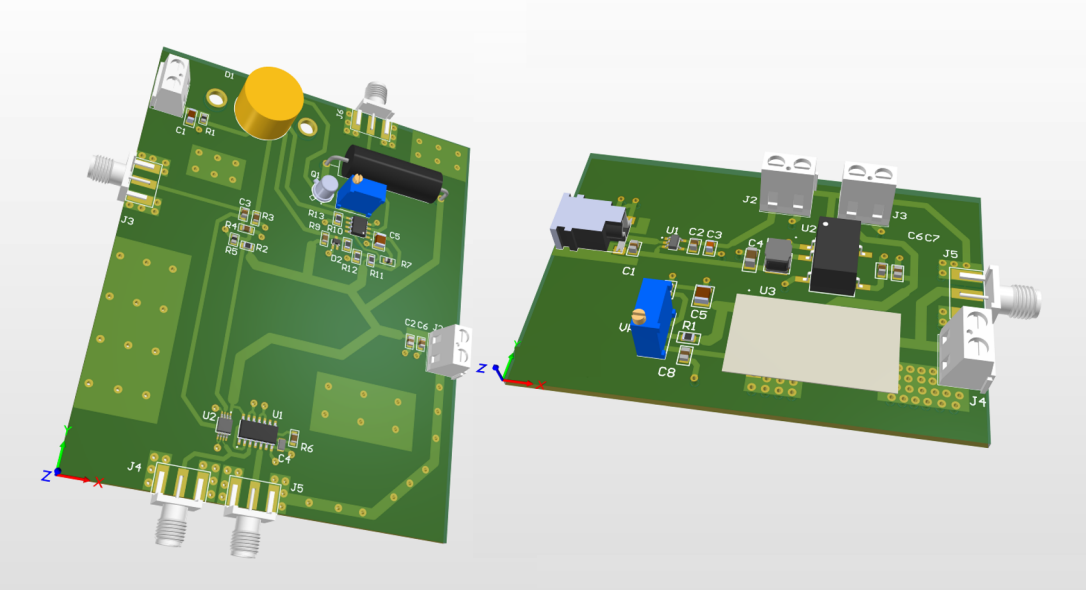

Figure 23: Mechanical drawing (left: quenching circuit, right: power circuit).

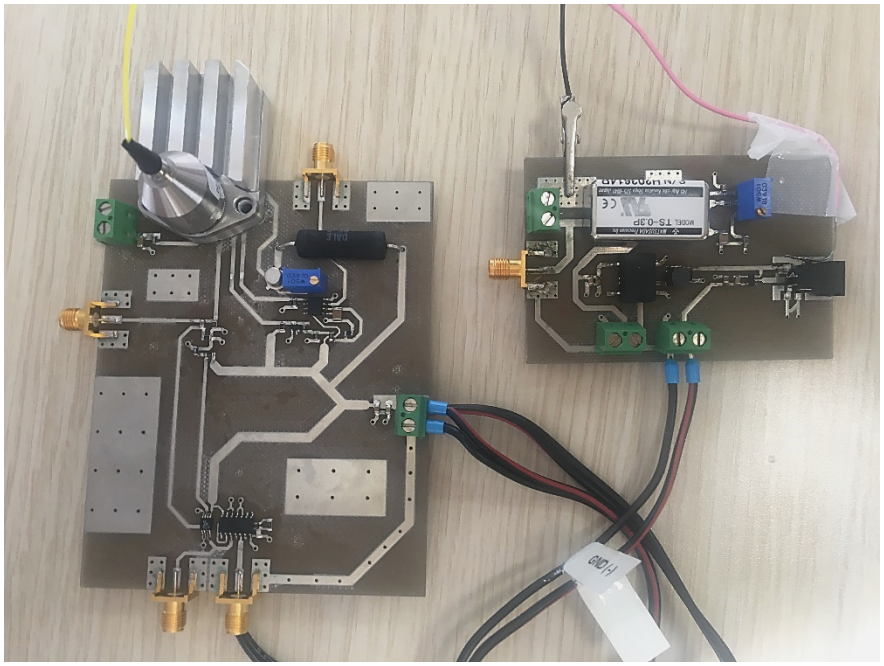

Figure 24: A photo of the single photon detection system.

CHAPTER IV

RESULTS AND DISCUSSION

This chapter serves as the cornerstone of exploration into single photon detection, providing a detailed analysis of outcomes derived from practical experimentation. This section bridges the theoretical concepts outlined in earlier chapters with the empirical realities encountered during investigations. Within this segment, various aspects were examined. The efficiency of the power supply was evaluated with its noise levels and the importance of the impact on the single photon detection system. Simultaneously, temperature controller performance was analyzed for different thermistor values since the effect of temperature on detector performance is a crucial focus. Controlled variations in temperature provide insights into how environmental conditions influence sensitivity, dark count rates, and overall efficiency. The single photon detection system was examined both with and without APD to understand how the surrounding electronics behave. The dark count rate, which is the inherent noise level of the detector in the absence of incident photons, was measured, and its usage for space applications was evaluated. Challenges encountered during experimental endeavors contributed to the refinement of methodologies.

4.1 Experimental Setup

The block diagram of the measurement setup is shown in Figure 25. In the PQ circuit with the temperature controller board, there are four outputs to measure the anode, the temperature, the comparator, the D flip flop, and two inputs for low voltage supply (5V DC), the bias (132V DC). The power supply board has three outputs for low voltage supplies (5V DC, 12V DC), the bias (132V DC), and an input for a direct connection to the grid. All measurement results were recorded on the Siglent SDS501

digital oscilloscope, and LG DC Power Supply GP-4303D was used as a power source. All measurements were conducted under standard room conditions.

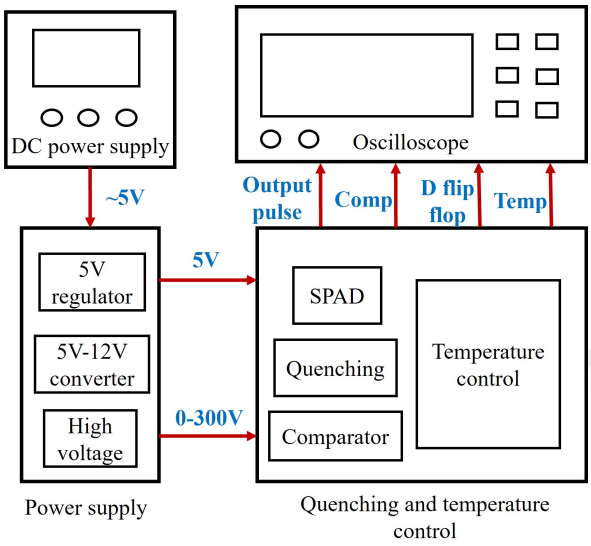

Figure 25: Setup for single photon detection system measurements.

4.2 Power Supply Board Analysis

Ensuring a clean DC output from the power supply board is very important for precise measurements with minimal noise interference, as discussed earlier. Although DC voltage theoretically has a frequency of 0, a harmonic component on DC from an AC source invariably exists. This unwanted noise is effectively filtered out using various electronic components. The significance of this filtration lies in mitigating several drawbacks, including signal integrity issues, decreased power supply efficiency, and accelerated equipment aging. In this study, strategic precautions have been adopted to enhance the quality of the power supply output. Decoupling capacitors have been strategically positioned alongside the power supplies to minimize the impact of noise. Furthermore, the inclusion of low-noise components, such as high voltage amplifiers exhibiting a ripple of less than 10 m$V_{peak-peak}$, has been instrumental in reducing the adverse effects of the harmonic component. These precautions contribute to creating a conducive environment for accurate and reliable measurements, diminishing the

influence of unwanted noise, and ensuring the overall integrity of the experimental setup. The power supply board is shown in Figure 26.

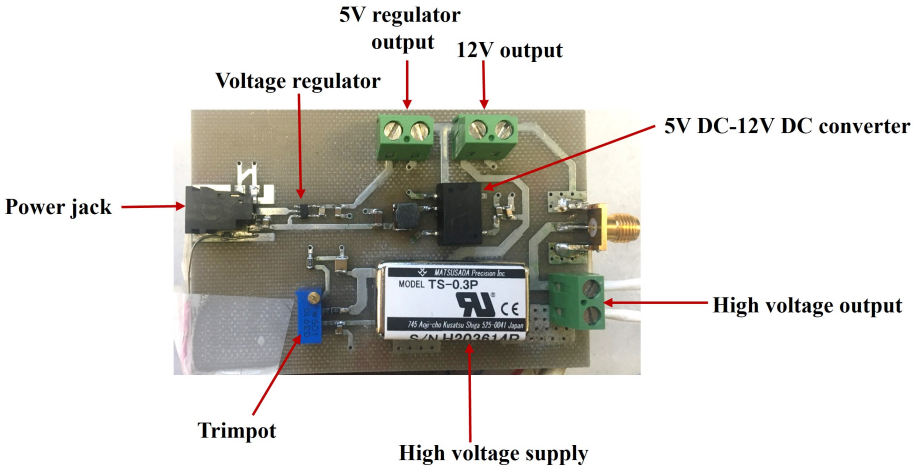

Figure 26: Power supply board.

An analysis of the ripple was conducted for the 5 V DC power input - 5 V DC regulator output and the 5 V DC regulator output - 132 V DC high voltage output using an oscilloscope with AC coupling to assess the operational characteristics of the DC sources integrated into the circuit board. In order to enhance precision during measurements, the V/div value was adjusted to a sufficiently small scale, facilitating the discernment of measurement values with high precision. Furthermore, the s/div value was set at a larger scale to capture the peak values of the AC voltage effectively. Since the ground loop formed by the return path of the probe results in an inductance that may both increase internal noise and subsequently amplify internal noise or capture external noise, measures were taken to connect the ground clip of the probe in close proximity to the signal source from which the ripple measurements were extracted. This strategic positioning aimed to reduce the negative impacts associated with ground loop formation and thus provide a more accurate representation of ripple characteristics. Figure 27 shows an oscilloscope display of the ripple measurement of the 5V power source and the 5V regulator output. Figure 28 shows an oscilloscope display of the ripple measurement of the 5V DC regulator output and 132V DC

high voltage output. The ripple of the 5V regulator output is approximately equal to 15 m$V_{peak-peak}$, the ripple of the 5V power source is approximately equal to 19 m$V_{peak-peak}$, and the ripple of the 132V DC is approximately equal to 69 m$V_{peak-peak}$. The noise level in the power supply for the high voltage output and the regulator output can be acceptable for this system, but changes in voltage levels may change the ripple level of the sources. On the other hand, the difference between the ripple of the 5V DC power input and the 5V DC regulator output was smaller than expected. This observed phenomenon may be attributed to the inherent characteristics of the 5V DC input, which is the output of the 220 V AC – 5V DC adapter. This adapter is inherently equipped with components designed to filter out undesirable noise effectively. In essence, the incoming signal to the circuit board maintains a clean DC state by noise-mitigated input to the subsequent circuitry.

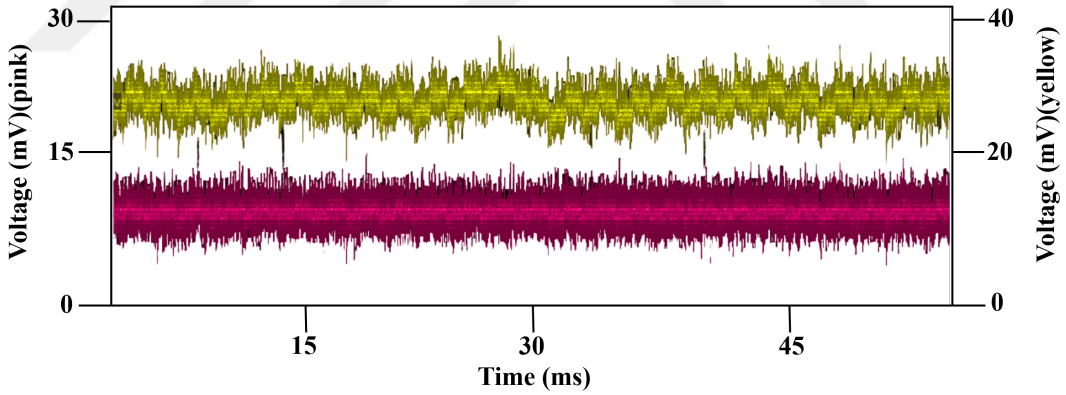

Figure 27: The ripple measurement (pink: 5V DC regulator, yellow: 5V DC).

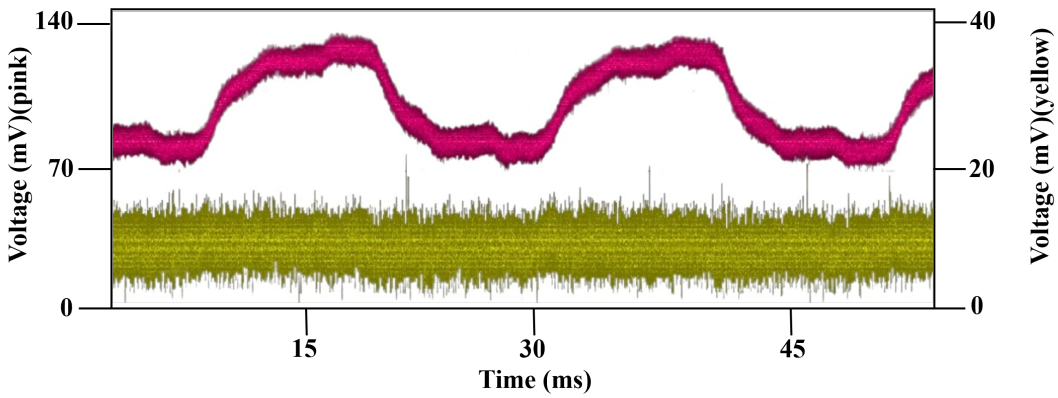

Figure 28: The ripple measurement (pink: 132V DC, yellow: 5V DC).

4.3 The Quenching with the Temperature Control Board Analysis

The quenching with the temperature control board is shown in Figure 29. Several experiments were conducted to thoroughly understand how well the single photon detection system works.

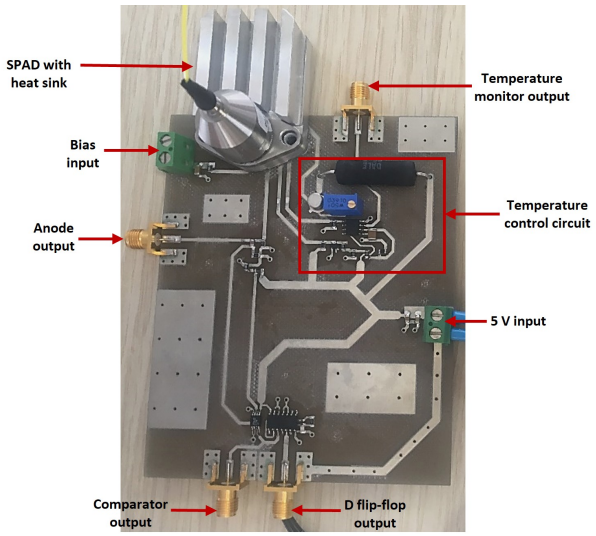

Figure 29: A photo of the quenching and temperature control board.

Before diving into the characterization of the SPAD, the circuit board without the APD was tested first. This initial step helped check how other parts of the system operate. The diagram illustrating the setup for these initial experiments is presented

in Figure 30. This groundwork was essential before delving into a more detailed examination of the SPAD, providing valuable insights into the overall performance dynamics of the entire single photon detection system.

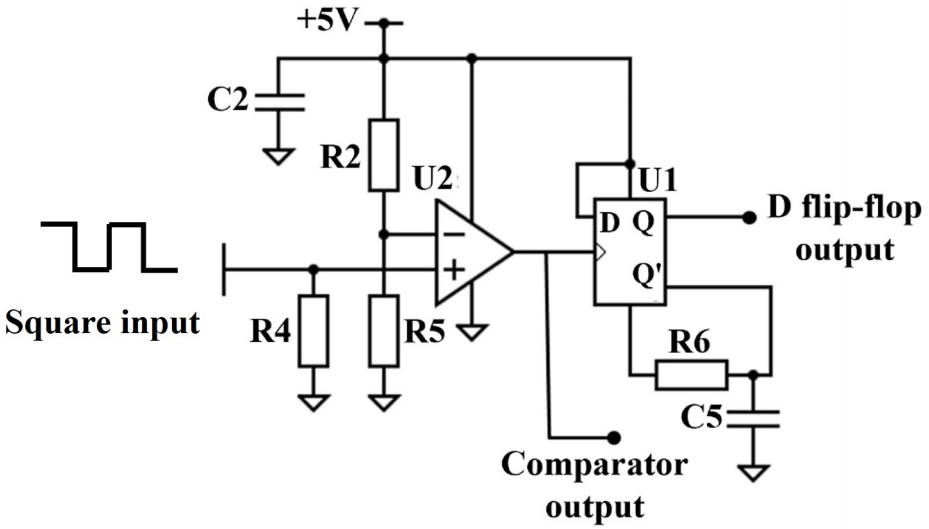

Figure 30: The schematic of the measurement circuit.

In this experiment, the square input was connected to the positive input of the comparator with a resistor. The pulse amplitude of the square input is increased from approximately 0 to 500 mV, and the pulses have a 50% duty cycle with a period of 1 ms. On the other hand, the negative input of the comparator has a constant reference value of 22 mV. Thus, half of the time, the positive input voltage is greater than the negative input voltage of the comparator in a period, while in the other half of the time, the negative input voltage is greater than the positive input voltage of the comparator in a period. Therefore, the comparator should output a waveform compatible with the square input because the comparator used gives "high" output, which is equal to the positive supply voltage if the positive voltage input is greater than the negative voltage input of the comparator and "low" output which is equal to the ground (GND) if the negative voltage input is greater than positive voltage input of the comparator. Figure 31 shows an oscilloscope display of the comparator output

with a square input. This result shows that the comparator can work properly when the avalanche effect starts and ends.

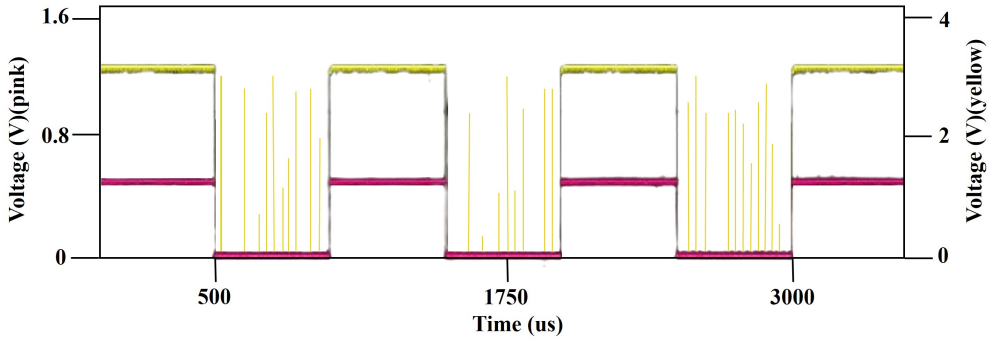

Figure 31: Oscilloscope image (yellow: comparator output, pink: square input).

On the other hand, some pulses were observed when the comparator was supposed to show a low output in the output waveform. Some transient pulses or external noise may lead to this problem. The Schmitt trigger circuit structure was implemented to address this issue, as shown in Figure 32, which significantly reduced the occurrence of such pulses. Despite this improvement, it is essential to note that using the Schmitt trigger circuit as a comparator for the SPAD has its challenges. The Schmitt trigger may introduce some delay in its response, and this delay can be a concern in applications like single photon detection, where timing precision is crucial [92]. As a result, the Schmitt trigger circuit was not used in subsequent experiments to avoid potential timing issues.

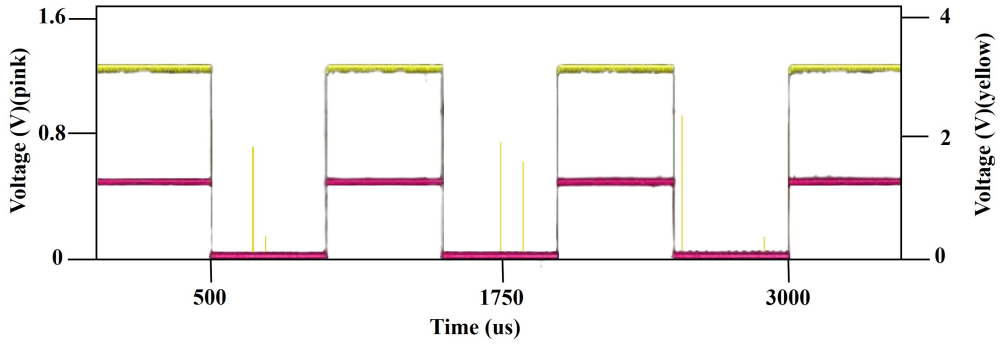

Figure 32: Oscilloscope image (yellow: Schmitt trigger, pink: square input).

In the second experiment, the D flip-flop and comparator outputs using a square input were measured. Figure 33 displays an oscilloscope image capturing these outputs. The results indicate that the D flip-flop consistently produces a high output when the comparator output is high, aligning with the intended outcome.

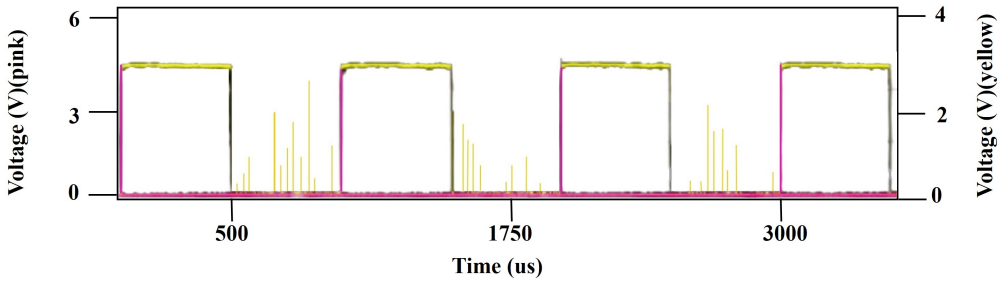

Figure 33: Oscilloscope image (yellow: comparator, pink: D flip-flop).

The third experiment was performed to inspect the temperature control of the SPAD with a potentiometer by using the TO-8 SAP500 series Si APD thermistor curve shown in Figure 13. The configuration of the experimental setup is shown in Figure 34.

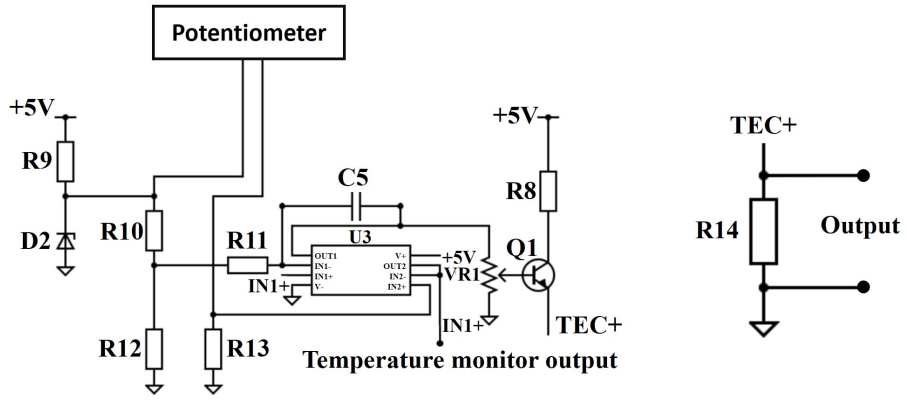

Figure 34: The schematic of the temperature control test circuit.

Within this experimental arrangement, the potentiometer functioned as a substitute for the internal thermistor within the SPAD. The resistance value of the potentiometer was adjusted to align with the resistance values characteristic of the thermistor. The temperature controller was analyzed for 308 K and 263 K. Figure 35 shows the oscilloscope display of the temperature monitor output (TMO) and the TEC output at 308 K, and Figure 36 shows the oscilloscope display of the TMO and the TEC output at 263 K. The THR of the APD at 308 K and 263 K equals 0.87 kΩ and 4.41 kΩ respectively. While temperature decreases, it was observed that the TMO output decreases from 58.3 m$V_{peak-peak}$ to 3.8 m$V_{peak-peak}$, and the TEC voltage increases from 41 m$V_{peak-peak}$ to 43.3 m$V_{peak-peak}$ [93].

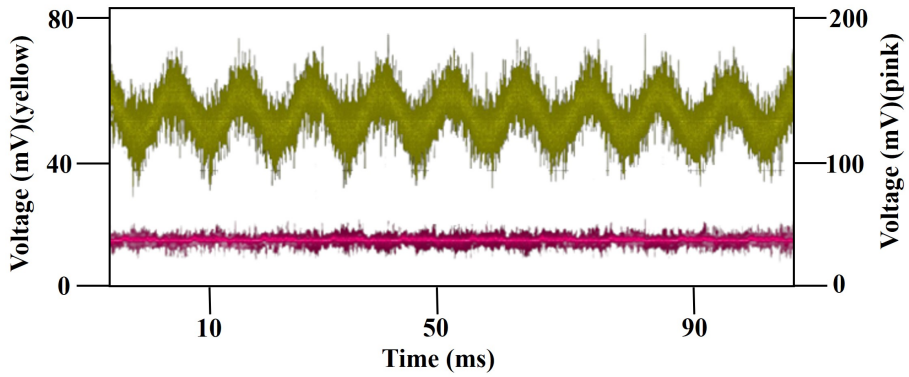

Figure 35: The TMO and TEC outputs at 308 K (pink: TMO, yellow: TEC).

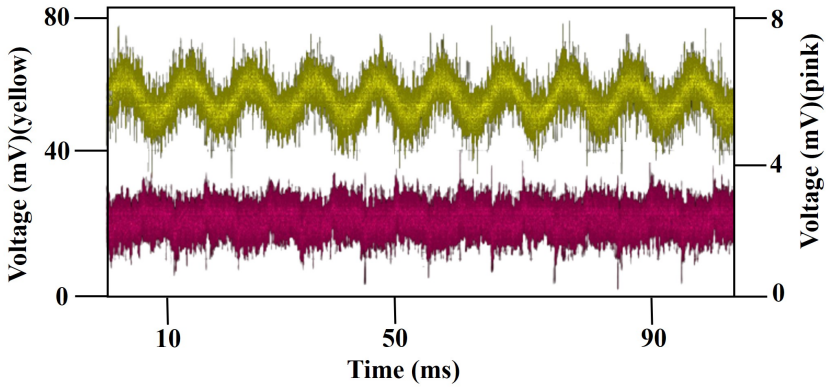

Figure 36: The TMO and TEC outputs at 263 K (pink: TMO, yellow: TEC).

Figure 37 shows an oscilloscope display of the anode output and D flip-flop output. As expected, the D flip-flop gave a less noisy and clear "high" output where the photon was detected. The anode output of the APD is approximately equal to 89 m$V_{peak-peak}$, and D flip-flop output is equal to 2.65 $V_{peak-peak}$. When the detector is operated in a dark environment, the dark count rate of the detector is approximately 2.5 kcps, as shown in the figure. This shows that the SPD was able to reach 278 K by the temperature controller. When the heat sink on the APD was removed, that is, when it was operated in a bright environment, only noise was detected. This may be due to the fact that outside the range of effective photon counting rates, passively quenched SPDs exhibit saturation and blinding properties. For SPDs, the count rate

rises nearly linearly with the intensity of continuous wave illumination. At higher light intensities, the count rate saturates and starts to drop [94].

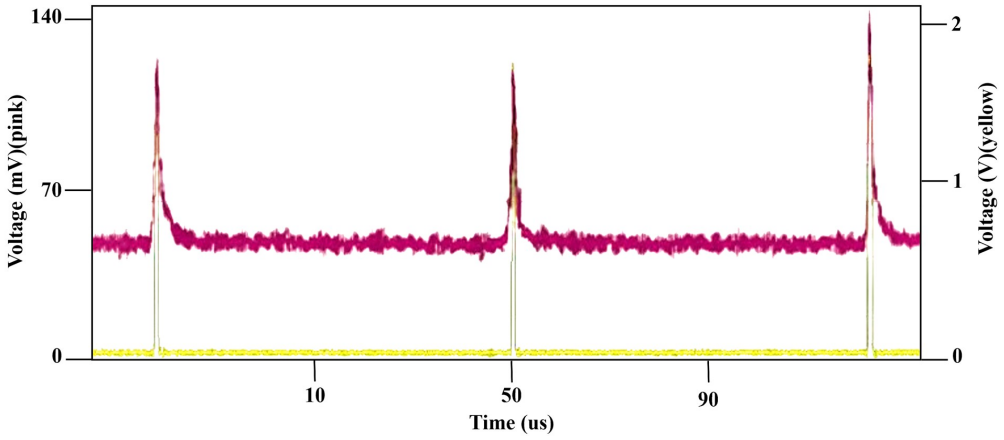

Figure 37: Oscilloscope image (pink: the anode, yellow: D flip-flop).

One of our motivations was to investigate the CubeSat compatibility of the detector. Solid state design, low operating voltage, absence of cooling [95], and high optical signal overload tolerance are attractive features for space applications. To simulate the solar flux, the laser diode with a beam of 5 mW power was used in experiments [96]. The beam was pointed onto a 500 µm diameter active area of the detector with a power of 1 mW due to 80% losses, and it was illuminated without applying any bias voltage for 1 hour. Experimental results showed that the solid-state detector could achieve a minimum dark counting rate of approximately 20 kHz when operated at a fixed voltage above breakdown (initially set at an excess voltage of 7V) while varying the temperature, and no degradation was observed after the illumination experiments. Figure 38 shows an oscilloscope display of the anode output and the comparator output, and Figure 39 shows a zoomed-in oscilloscope display of the anode output and comparator output [93].

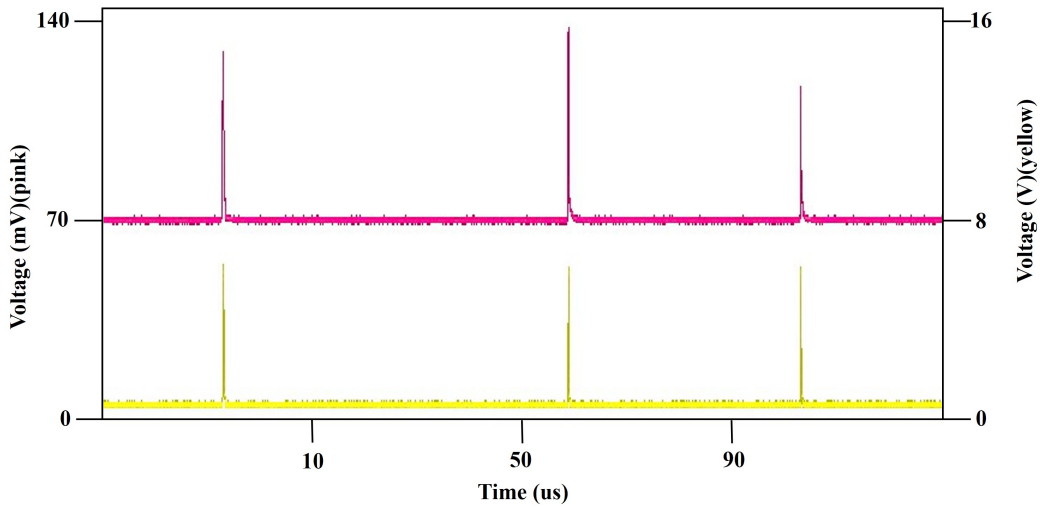

Figure 38: Oscilloscope image (pink: anode, yellow: comparator).

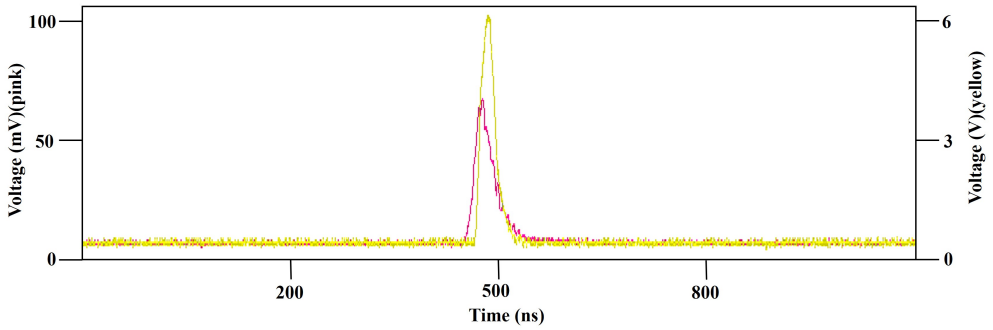

Figure 39: A zoomed-in display (pink: anode, yellow: comparator).

In the later stages of the design, more decoupling capacitors can be used to enhance the power section in the temperature-controlled quenching circuit. This strategic addition serves to deliver a supply voltage characterized by reduced noise, contributing to the overall stability and accuracy of the single photon detection system. Similarly, a Schottky diode can be used to prevent the risk of reverse connection of the "-" and "+" ends of the two-position connectors positioned for power supplies. Furthermore, the application of a current limiter can also be used as a protective measure to protect the APD from possible damage caused by excessive current draw. An optimization strategy can involve distributing power signals across multiple ground pins instead of relying on a single pin, facilitating more efficient signal transmission. The power

inputs of the components can be additionally filtered by placing a ferrite bead on the power supply inputs, further enhancing the reliability of the power supply. Additionally, "solder bridges" can be placed in the areas where the power inputs are located. First, it is checked whether the correct voltage can be measured from the connector, then the solder bridge is lined up, and card testing begins. The GNDs to which the analog signal and the digital signal are referenced can be separated from each other using ferried beads. In this way, the adverse effects of noise occurring in the digital part on analog signals can be minimized. Lastly, minimizing error margins can be achieved through the selection of components with lower tolerances for resistances and capacities, ensuring precision in the functioning of the experimental setup.

More low-pass filters can be placed on the power inputs and outputs on the power card. Since the power card is planned to be used as a generic card, possible power consumption scenarios can be determined, and a fuse can be used to prevent the possibility of damage caused by overcurrent. LEDs for 12V and 5V can be put into operation to control the status of the supply sources. In this way, in case of a possible problem with the quenching card, it can be understood whether there is a power problem from the status LEDs instead of measuring the supply sources one by one with the measuring instrument. Although the +5V DC output on the power board has a wide input range (1.8V to 20V), the +12V DC output does not have a wide input range (4.5V to 5.5V). A DC-DC converter with a wider input range can be selected, thus providing a wider selection spectrum for the adapter to be installed on the card. The SMA output, which is placed as an extra for high voltage output on the power card, is intended to be used for oscilloscope tracking. However, the DC inputs of oscilloscopes are generally 5V root mean square (RMS) for the 50ohm termination probe. Therefore, this connector could not be used, and this connector should be removed from the design in future studies.

Some improvements can also be made in the PCB drawings section. These cards

manufactured are 2-layers. Reducing the size of the card may be mechanically better and more useful, so the number of layers can be increased to 4-layers. Also, component placements can be made more strategically, resulting in a more efficient area. Afterward, the GND polygon should be added to all layers, and GND stitching should be done with vias. Additionally, important signals such as the APD signal can be carried via GND vias. This provides better operation for electromagnetic interference/electromagnetic compatibility (EMI/EMC) and signal integrity. Similarly, the corners of the polygons can be softened to prevent them from behaving like antennas.

When considered for each card, having "test points" on the cards makes it easier to test the cards. For places where input/output (I/O) pins other than VCC and GND must be "high" and "low" on integrated circuits, "pull-up" and "pull-down" configurations can be used by connecting them with resistors rather than connecting them directly to VCC or GND. This introduces current limiting to the respective pins, offering a safeguard against excessive current. In instances where the design is uncertain or alternative design topologies have been experimentally tried, 0Ω resistors can be strategically employed. This approach allows for flexible design modifications, whether or not implemented 0Ω resistors, providing adaptability to refine the configuration of the circuit. In addition, screw holes can be placed on the cards for chassis, and these chassis are connected to GND using capacitors, and the noise on GND can be grounded from the mechanics where the card is positioned. Another important issue is "Bill of material (BOM) optimization". Instead of resistors and capacitors with similar values, resistors, and capacitors of the same value can be preferred if they do not cause a critical change in the design. This can both reduce costs and speed up purchasing, tracking, and card sorting processes. Finally, the cards can undergo prolonged operation with suitable measuring instruments, undergoing comprehensive hot-cold and vibration tests. Analyzing detailed data on hourly current draw periods and heating rates ensures a thorough assessment of the performance of cards over an

extended operational duration.

CHAPTER V

CONCLUSIONS

In conclusion, the design and implementation of SPDs represent a very significant advance in the field of photonics and quantum technologies. One of the main focuses of this research has been to investigate and highlight the role of single photon detectors in this field. Detecting coincidences between entangled photons opens avenues for quantum computing, QKD, and other quantum communication protocols. The findings underscore the importance of SPDs in pushing the boundaries of quantum technologies and determining their viability in the emerging quantum era. Moreover, it is noteworthy that the impact of SPDs extends far beyond the quantum information domain. The versatility of these detectors positions them as valuable tools for a wide variety of applications, including communications, depth measurement, sensing, and integrated circuit testing. Although significant progress has been made, it is important to acknowledge the challenges encountered in the design and implementation of SPDs. Technological limitations, experimental complexities, and the need for further improvements in efficiency and reliability offer avenues for future research. Researching new materials, optimizing production processes, and discovering new detection mechanisms are important steps toward improving the performance of these detectors. Interdisciplinary cooperation is necessary for the integration of SPDs into useful devices and systems. Realizing the complete potential of these detectors will depend on bridging the knowledge gap between theoretical advancements and real-world applications. In addition to improving existing designs, future research efforts should concentrate on exploring novel methodologies that could lead to developing next-generation detectors with enhanced capabilities. In this thesis, the SPD

design as a driving circuit of the TO-8 SAP500 series Silicon APD provided by Laser Component has been proposed. The comprehensive presentation of the PQ circuit, including detailed designs for both the temperature controller and power supply circuits, has been meticulously provided. An examination of the power supply has been conducted to analyze ripples, enabling a noise analysis for enhanced understanding. The temperature controller, an integral component of the system, has been assessed for its performance, with the capability of the SPD reaching a temperature of 278 K. An inspection of the power supply was carried out to assess noise levels, establishing that they remain within acceptable parameters for the effective functioning of the overall system. Simultaneously, the performance of the temperature controller has been evaluated as adequate, contributing to the operational stability and efficiency of the system. The research involved a comprehensive analysis of the single photon detection system under two conditions: with and without APD. This investigation aimed to comprehend the behavior of the surrounding electronics in both scenarios. The dark count rate, representing the inherent noise level of the detector, was measured. Additionally, an evaluation was made regarding its potential use in space-related applications. Furthermore, an exploration into the performance characteristics and spatial compatibility of the SPD has been investigated. Operational behavior at low voltages, low mass, capability to maintain a low dark count rate even without the necessity of cooling mechanisms, and high optical signal overload tolerance for TO-8 SAP500 APD are attractive features that enhance its suitability for applications requiring robust performance under varying optical input conditions. These appealing attributes collectively contribute to positioning it as an attractive choice, promising versatility and efficiency in diverse operational settings.

APPENDIX A

COMPONENT LIST

Table 1: Component List of the Power Card

No	Designator	Description
1	R1	RES SMD 10K OHM 0.1% 1/8W 0805
2	R2	RES SMD 10K OHM 0.1% 1/8W 0805
3	VR1	TRIMMER 20K OHM 0.5W PC PIN TOP
4	C1	CAP CER 1UF 50V X7R 0805
5	C2	CAP CER 10000PF 50V X7R 0805
6	C3	CAP CER 10UF 25V X5R 0805
7	C4	CAP CER 4.7UF 50V X7R 0805
8	C5	CAP CER 2.2UF 50V X7R 1210
9	C6	CAP CER 10000PF 50V X7R 0805
10	C7	CAP CER 0.1UF 50V X7R 0805
11	C8	CAP CER 0.1UF 50V X7R 0805
12	J1	CONN PWR JACK 1.70X4.75MM SOLDER
13	J2	TERM BLK 2P SIDE ENT 5.08MM PCB
14	J3	TERM BLK 2P SIDE ENT 5.08MM PCB
15	J4	TERM BLK 2P SIDE ENT 5.08MM PCB
16	J5	CONN SMA RCPT STR 50OHM EDGE MNT
17	U1	IC REG LINEAR 5V 100MA TSOT23-5
18	U2	DC DC CONVERTER 12V 1W
19	U3	MATSUSADA TS-0.3P
20	L1	FIXED IND 6.8UH 3A 39 MOHM SMD

Table 2: Component List of the Quenching Card with the Temperature Controller

No	Designator	Description
1	R1	RES 560K OHM 1% 1/8W 0805
2	R2	RES 22K OHM 1% 1/8W 0805
3	R3	RES SMD 220 OHM 1% 1/8W 0805
4	R4	RES SMD 470 OHM 5% 1/8W 0805
5	R5	RES 100 OHM 1% 1/8W 0805
6	R6	RES SMD 220 OHM 1% 1/8W 0805
7	R8	RES 10 OHM 5W 1% WW AXIAL
8	R9	RES SMD 470 OHM 5% 1/8W 0805
9	R10	RES 6.8K OHM 1% 1/8W 0805
10	R11	RES 200K OHM 1% 1/8W 0805
11	R12	RES 6.8K OHM 1% 1/8W 0805
12	R13	RES 6.8K OHM 1% 1/8W 0805
13	VR1	TRIMMER 20K OHM 0.5W PC PIN TOP
14	C1	CAP CER 0.1UF 250V X7R 1812
15	C2	CAP CER 0.1UF 50V X7R 0805
16	C3	CAP CER 100PF 100V C0G/NP0 0805
17	C4	CAP CER 200PF 50V NP0 0805
18	C5	CAP CER 2.2UF 50V X7R 1210
19	C6	CAP CER 0.1UF 50V X7R 0805
20	C7	CAP CER 0.1UF 50V X7R 0805
21	J1	TERM BLK 2P SIDE ENT 5.08MM PCB
22	J2	TERM BLK 2P SIDE ENT 5.08MM PCB
23	J3	CONN SMA RCPT STR 50OHM EDGE MNT
24	J4	CONN SMA RCPT STR 50OHM EDGE MNT
25	J5	CONN SMA RCPT STR 50OHM EDGE MNT
26	J6	CONN SMA RCPT STR 50OHM EDGE MNT
27	U1	IC FF D-TYPE DUAL 1BIT 14SOIC
28	U2	IC COMPARATOR 1 W/LATCH 8MSOP
29	U3	IC OPAMP GP 2 CIRCUIT 8SOIC
30	D1	LASER COMPONENTS TO-8 SAP500
31	D2	DIODE ZENER 3.3V 500MW TUMD2M
32	Q1	TRANS NPN 40V 0.8A TO18

REFERENCES

[1] M. Stipčević, H. Skenderović, and D. Gracin, "Characterization of a novel avalanche photodiode for single photon detection in vis-nir range," *Optics express*, vol. 18, no. 16, pp. 17448–17459, 2010.

[2] L.-Q. Li and L. M. Davis, "Single photon avalanche diode for single molecule detection," *Review of Scientific Instruments*, vol. 64, no. 6, pp. 1524–1529, 1993.

[3] B. Levine, C. Bethea, L. Cohen, J. Campbell, and G. Morris, "Optical time domain reflectometer using a photon-counting ingaas/inp avalanche photodiode at 1.3 μm," *Electronics Letters*, vol. 2, no. 21, pp. 83–84, 1985.

[4] W. Becker, A. Bergmann, M. Hink, K. König, K. Benndorf, and C. Biskup, "Fluorescence lifetime imaging by time-correlated single-photon counting," *Microscopy research and technique*, vol. 63, no. 1, pp. 58–66, 2004.

[5] J. Bouchard, A. Samson, W. Lemaire, C. Paulin, J.-F. Pratte, Y. Bérubé-Lauzière, and R. Fontaine, "A low-cost time-correlated single photon counting system for multiview time-domain diffuse optical tomography," *IEEE Transactions on Instrumentation and Measurement*, vol. 66, no. 10, pp. 2505–2515, 2017.

[6] B. Schuler, "Application of single molecule förster resonance energy transfer to protein folding," *Protein Folding Protocols*, pp. 115–138, 2006.

[7] E. Reiger, S. Dorenbos, V. Zwiller, A. Korneev, G. Chulkova, I. Milostnaya, O. Minaeva, G. Gol'tsman, J. Kitaygorsky, D. Pan, *et al.*, "Spectroscopy with nanostructured superconducting single photon detectors," *IEEE Journal of Selected Topics in Quantum Electronics*, vol. 13, no. 4, pp. 934–943, 2007.

[8] C. Yu, M. Shangguan, H. Xia, J. Zhang, X. Dou, and J.-W. Pan, "Fully integrated free-running ingaas/inp single-photon detector for accurate lidar applications," *Optics express*, vol. 25, no. 13, pp. 14611–14620, 2017.

[9] T. Isoshima, Y. Isojima, K. Hakomori, K. Kikuchi, K. Nagai, and H. Nakagawa, "Ultrahigh sensitivity single-photon detector using a si avalanche photodiode for the measurement of ultraweak biochemiluminescence," *Review of scientific instruments*, vol. 66, no. 4, pp. 2922–2926, 1995.

[10] F. Stellari, A. J. Weger, S. Kim, D. Maliuk, P. Song, H. A. Ainspan, Y. Kwark, C. W. Baks, U. Kindereit, V. Anant, *et al.*, "A superconducting nanowire single-photon detector (snspd) system for ultra low voltage time-resolved emission (tre) measurements of vlsi circuits," in *Int. Symp. for Testing and Failure Analysis (ISTFA)*, pp. 182–188, 2013.

[11] Q. Yan, Z. Li, Z. Hong, T. Zhan, and Y. Wang, "Photon-counting underwater wireless optical communication by recovering clock and data from discrete single photon pulses," *IEEE Photonics Journal*, vol. 11, no. 5, pp. 1–15, 2019.

[12] G. Gudkov, V. Dhulla, A. Borodin, D. Gavrilov, A. Stepukhovich, A. Tsupryk, B. Gorbovitski, and V. Gorfinkel, "32-channel single photon counting module for ultrasensitive detection of dna sequences," in *Advanced Photon Counting Techniques*, vol. 6372, pp. 91–96, SPIE, 2006.

[13] T. Staffas, "Live 3d imaging quantum lidar," 2021.

[14] W. contributors, "Photomultiplier tube," 2022. Online; accessed 09-March-2022.

[15] H. Hertz, "Ueber einen einfluss des ultravioletten lichtes auf die electrische entladung," *Annalen der Physik*, vol. 267, no. 8, pp. 983–1000, 1887.

[16] J. Elster and H. Geitel, "Ueber die entladung negativ electrischer körper durch das sonnen-und tageslicht," *Annalen der Physik*, vol. 274, no. 12, pp. 497–514, 1889.

[17] J. Elster and H. Geitel, "Ueber die vergleichung von lichtstärken auf photoelectrischem wege," *Annalen der Physik*, vol. 284, no. 4, pp. 625–635, 1893.

[18] M. D. Eisaman, J. Fan, A. Migdall, and S. V. Polyakov, "Invited review article: Single-photon sources and detectors," *Review of scientific instruments*, vol. 82, no. 7, p. 071101, 2011.

[19] B. K. Lubsandorzhiev, "On the history of photomultiplier tube invention," *Nuclear Instruments and Methods in Physics Research Section A: Accelerators, Spectrometers, Detectors and Associated Equipment*, vol. 567, no. 1, pp. 236–238, 2006.

[20] D. Renker, "Geiger-mode avalanche photodiodes, history, properties and problems," *Nuclear Instruments and Methods in Physics Research Section A: Accelerators, Spectrometers, Detectors and Associated Equipment*, vol. 567, no. 1, pp. 48–56, 2006.

[21] W. contributors, "Pin diode," 2022. Online; accessed 10-December-2023.

[22] R. McIntyre, "Theory of microplasma instability in silicon," *Journal of Applied Physics*, vol. 32, no. 6, pp. 983–995, 1961.

[23] R. H. Haitz, "Model for the electrical behavior of a microplasma," *Journal of Applied Physics*, vol. 35, no. 5, pp. 1370–1376, 1964.

[24] W. contributors, "Avalanche photodiode," 2022. Online; accessed 22-June-2022.

[25] F. Zappa, A. Lotito, A. C. Giudice, S. Cova, and M. Ghioni, "Monolithic active-quenching and active-reset circuit for single-photon avalanche detectors," *IEEE Journal of Solid-State Circuits*, vol. 38, no. 7, pp. 1298–1301, 2003.

[26] S. Cova, M. Ghioni, A. Lotito, I. Rech, and F. Zappa, "Evolution and prospects for single-photon avalanche diodes and quenching circuits," *Journal of modern optics*, vol. 51, no. 9-10, pp. 1267–1288, 2004.

[27] R. H. Hadfield, "Single-photon detectors for optical quantum information applications," *Nature photonics*, vol. 3, no. 12, pp. 696–705, 2009.

[28] A. Tosi, A. D. Mora, F. Zappa, and S. Cova, "Single-photon avalanche diodes for the near-infrared range: detector and circuit issues," *Journal of Modern Optics*, vol. 56, no. 2-3, pp. 299–308, 2009.

[29] C. M. Natarajan, M. G. Tanner, and R. H. Hadfield, "Superconducting nanowire single-photon detectors: physics and applications," *Superconductor science and technology*, vol. 25, no. 6, p. 063001, 2012.

[30] H. KAMERLINGH, "Further experiments with liquid helium. c. on the change of electric resistance of pure metals at very low temperatures, etc. iv. the resistance of pure mercury at helium temperatures," *Comm. Phys. Lab. Univ. Leiden*, vol. 120, pp. 261–263, 1911.

[31] G. Gol'Tsman, O. Okunev, G. Chulkova, A. Lipatov, A. Semenov, K. Smirnov, B. Voronov, A. Dzardanov, C. Williams, and R. Sobolewski, "Picosecond superconducting single-photon optical detector," *Applied physics letters*, vol. 79, no. 6, pp. 705–707, 2001.

[32] E. A. Dauler, M. E. Grein, A. J. Kerman, F. Marsili, S. Miki, S. W. Nam, M. D. Shaw, H. Terai, V. B. Verma, and T. Yamashita, "Review of superconducting nanowire single-photon detector system design options and demonstrated performance," *Optical Engineering*, vol. 53, no. 8, pp. 081907–081907, 2014.

[33] L. You, "Superconducting nanowire single-photon detectors for quantum information," *Nanophotonics*, vol. 9, no. 9, pp. 2673–2692, 2020.

[34] S. Quantum, "The top-notch of light detection: Snspds," n.d. Accessed: 12-September-2022.

[35] S. Cherednichenko, N. Acharya, E. Novoselov, and V. Drakinskiy, "Ir-and visible-light single photon detection in superconducting *mgb_*{2} nanowires," *arXiv preprint arXiv:1911.01652*, 2019.

[36] T. Yamashita, S. Miki, and H. Terai, "Recent progress and application of superconducting nanowire single-photon detectors," *IEICE Transactions on Electronics*, vol. 100, no. 3, pp. 274–282, 2017.

[37] H. Weier, H. Krauss, M. Rau, M. Fürst, S. Nauerth, and H. Weinfurter, "Quantum eavesdropping without interception: an attack exploiting the dead time of single-photon detectors," *New Journal of Physics*, vol. 13, no. 7, p. 073024, 2011.

[38] H. Georgieva, A. Meda, S. M. Raupach, H. Hofer, M. Gramegna, I. P. Degiovanni, M. Genovese, M. López, and S. Kück, "Detection of ultra-weak laser pulses by free-running single-photon detectors: modeling dead time and dark counts effects," *Applied Physics Letters*, vol. 118, no. 17, p. 174002, 2021.

[39] J. Y. Cheung, C. J. Chunnilall, P. J. Thomas, J. R. Mountford, and N. P. Fox, "Photon counting: measurement challenges," in *Photon Counting Applications, Quantum Optics, and Quantum Cryptography*, vol. 6583, pp. 153–164, SPIE, 2007.

[40] R. G. Brown, K. D. Ridley, and J. G. Rarity, "Characterization of silicon avalanche photodiodes for photon correlation measurements. 1: Passive quenching," *Applied optics*, vol. 25, no. 22, pp. 4122–4126, 1986.

[41] S. Burgess and I. Shepherd, "Fluorescence suppression in time-resolved raman spectra," *Journal of physics E: Scientific instruments*, vol. 10, no. 6, p. 617, 1977.

[42] Y. Liang, B. Xu, Q. Fei, W. Wu, X. Shan, K. Huang, and H. Zeng, "Low-timing-jitter ghz-gated ingaas/inp single-photon avalanche photodiode for lidar," *IEEE Journal of Selected Topics in Quantum Electronics*, vol. 28, no. 2: Optical Detectors, pp. 1–7, 2021.

[43] R. J. Collins, R. Hadfield, V. Fernandez, S. W. Nam, and G. S. Buller, "Low timing jitter detector for gigahertz quantum key distribution," *Electronics Letters*, vol. 43, no. 3, pp. 180–182, 2007.

[44] L. Components, "Sap-series silicon geiger mode avalanche photodiode," n.d. Accessed: 23-May-2022.

[45] N. Gisin and G. Ribordy, "W. tittel i h. zbidnen," *Quantum cryptography, Rev. Mod. Phys*, vol. 74, p. 145, 2002.

[46] L. Z. Jie and C. Kurtsiefer, "Characterisation of single photon avalanche detectors," *Undergraduate Final Year Project Thesis, National University of Singapore*, 2016.

[47] R. C. Jone, "Quantum efficiency of detectors for visible and infrared radiation," *Advances in electronics and electron physics*, vol. 11, pp. 87–183, 1959.

[48] Hamamatsu, "About pmts: Photomultiplier tubes (pmts)," n.d. Accessed: 23-August-2022.

[49] Thorlabs, "Pmt2101 - gaasp amplified pmt," n.d. Accessed: 23-August-2022.

[50] Hamamatsu, "R5509-73," n.d. Accessed: 23-August-2022.

[51] Hamamatsu, "Photon counting head h12775," n.d. Accessed: 23-Aug-2022.

[52] Hamamatsu, "Si apd," n.d. Accessed: 23-Aug-2022.

[53] Hamamatsu, "Spad module," n.d. Accessed: 23-Aug-2022.

[54] Hamamatsu, "Spad modules," n.d. Accessed: 24-Aug-2022.

[55] MPD, "Fast gated-spad," n.d. Accessed: 24-Aug-2022.

[56] Thorlabs, "Spcm20a - single photon counting module," n.d. Accessed: 23-August-2022.

[57] Thorlabs, "Si avalanche photodetectors," n.d. Accessed: 23-August-2022.

[58] Hamamatsu, "Ingaas photodiodes," n.d. Accessed: 23-August-2022.

[59] IDQ, "Id281 superconducting nanowire," n.d. Accessed: 24-Aug-2022.

[60] C. C.-W. Lim and C. Wang, "Long-distance quantum key distribution gets real," *Nature Photonics*, vol. 15, no. 8, pp. 554–556, 2021.

[61] R. H. Hadfield, J. L. Habif, J. Schlafer, R. E. Schwall, and S. W. Nam, "Quantum key distribution at 1550nm with twin superconducting single-photon detectors," *Applied physics letters*, vol. 89, no. 24, p. 241129, 2006.

[62] A. Pljonkin, K. Rumyantsev, and P. Kumar Singh, "Synchronization in quantum key distribution systems," *Cryptography*, vol. 1, no. 3, p. 18, 2017.

[63] I. Takai, H. Matsubara, M. Soga, M. Ohta, M. Ogawa, and T. Yamashita, "Single-photon avalanche diode with enhanced nir-sensitivity for automotive lidar systems," *Sensors*, vol. 16, no. 4, p. 459, 2016.

[64] R. H. Hadfield, M. J. Stevens, R. P. Mirin, and S. W. Nam, "Single-photon source characterization with twin infrared-sensitive superconducting single-photon detectors," *Journal of Applied Physics*, vol. 101, no. 10, p. 103104, 2007.

[65] R. Alléaume, F. Treussart, J.-M. Courty, and J.-F. Roch, "Photon statistics characterization of a single-photon source," *New Journal of physics*, vol. 6, no. 1, p. 85, 2004.

[66] F. Madonini and F. Villa, "Single photon avalanche diode arrays for time-resolved raman spectroscopy," *Sensors*, vol. 21, no. 13, p. 4287, 2021.

[67] J. L. Lagarto, C. Credi, F. Villa, S. Tisa, F. Zappa, V. Shcheslavskiy, F. S. Pavone, and R. Cicchi, "Multispectral depth-resolved fluorescence lifetime spectroscopy using spad array detectors and fiber probes," *Sensors*, vol. 19, no. 12, p. 2678, 2019.

[68] K. Taguchi and J. S. Iwanczyk, "Vision 20/20: single photon counting x-ray detectors in medical imaging," *Medical physics*, vol. 40, no. 10, p. 100901, 2013.

[69] R. Ota, "Photon counting detectors and their applications ranging from particle physics experiments to environmental radiation monitoring and medical imaging," *Radiological Physics and Technology*, vol. 14, no. 2, pp. 134–148, 2021.

[70] Y. Seo, C. Mari, and B. H. Hasegawa, "Technological development and advances in single-photon emission computed tomography/computed tomography," in *Seminars in nuclear medicine*, vol. 38, pp. 177–198, Elsevier, 2008.

[71] B. R. Rae, C. Griffin, K. R. Muir, J. M. Girkin, E. Gu, D. R. Renshaw, E. Charbon, M. D. Dawson, and R. K. Henderson, "A microsystem for time-resolved fluorescence analysis using cmos single-photon avalanche diodes and micro-leds," in *2008 IEEE International Solid-State Circuits Conference-Digest of Technical Papers*, pp. 166–603, IEEE, 2008.

[72] D. Stoppa, L. Pancheri, M. Scandiuzzo, L. Gonzo, G.-F. Dalla Betta, and A. Simoni, "A cmos 3-d imager based on single photon avalanche diode," *IEEE Transactions on Circuits and Systems I: Regular Papers*, vol. 54, no. 1, pp. 4–12, 2007.

[73] T. Gerrits, S. Allman, D. J. Lum, V. Verma, J. Howell, R. Mirin, and S. W. Nam, "Progress toward a high-resolution single-photon camera based on superconducting single photon detector arrays and compressive sensing," in *CLEO: Science and Innovations*, pp. STh3O–6, Optica Publishing Group, 2015.

[74] M. Yang, F. Xu, J.-G. Ren, J. Yin, Y. Li, Y. Cao, Q. Shen, H.-L. Yong, L. Zhang, S.-K. Liao, *et al.*, "Spaceborne, low-noise, single-photon detection for satellite-based quantum communications," *Optics express*, vol. 27, no. 25, pp. 36114–36128, 2019.

[75] E. Anisimova, B. L. Higgins, J.-P. Bourgoin, M. Cranmer, E. Choi, D. Hudson, L. P. Piche, A. Scott, V. Makarov, and T. Jennewein, "Mitigating radiation damage of single photon detectors for space applications," *EPJ Quantum Technology*, vol. 4, pp. 1–14, 2017.

[76] M. E. Grein, A. J. Kerman, E. A. Dauler, O. Shatrovoy, R. J. Molnar, D. Rosenberg, J. Yoon, C. E. DeVoe, D. V. Murphy, B. S. Robinson, *et al.*, "Design of a ground-based optical receiver for the lunar laser communications demonstration," in *2011 International Conference on Space Optical Systems and Applications (ICSOS)*, pp. 78–82, IEEE, 2011.

[77] C. Natarajan, A. Peruzzo, S. Miki, M. Sasaki, Z. Wang, B. Baek, S. Nam, R. Hadfield, and J. L. O'Brien, "Operating quantum waveguide circuits with superconducting single-photon detectors," *Applied Physics Letters*, vol. 96, no. 21, p. 211101, 2010.

[78] R. E. Warburton, A. McCarthy, A. M. Wallace, S. Hernandez-Marin, R. H. Hadfield, S. W. Nam, and G. S. Buller, "Subcentimeter depth resolution using a single-photon counting time-of-flight laser ranging system at 1550 nm wavelength," *Optics letters*, vol. 32, no. 15, pp. 2266–2268, 2007.

[79] S. D. Dyer, M. G. Tanner, B. Baek, R. H. Hadfield, and S. W. Nam, "Analysis of a distributed fiber-optic temperature sensor using single-photon detectors," *Optics express*, vol. 20, no. 4, pp. 3456–3466, 2012.

[80] J. B. Abshire, H. Riris, G. Allan, X. Sun, S. R. Kawa, J.-P. Mao, M. Stephen, E. Wilson, and M. A. Krainak, "Laser sounder for global measurement of co2 concentrations in the troposphere from space," in *Laser Applications to Chemical, Security and Environmental Analysis*, p. LMA4, Optica Publishing Group, 2008.

[81] J. Zhang, N. Boiadjieva, G. Chulkova, H. Deslandes, G. Gol'Tsman, A. Korneev, P. Kouminov, M. Leibowitz, W. Lo, R. Malinsky, *et al.*, "Noninvasive cmos circuit testing with nbn superconducting single-photon detectors," *Electronics Letters*, vol. 39, no. 14, p. 1, 2003.

[82] W. contributors, "Photodiode," 2023. Online; accessed 13-December-2023.

[83] Neon, "What is the difference between a pin photodiode and a pn photodiode?," n.d. Accessed: 13-December-2023.

[84] M. Bakowski and I. Lundström, "Calculation of avalanche breakdown voltage and depletion layer thickness in a p- n junction with a double error function doping profile," *Solid-State Electronics*, vol. 16, no. 5, pp. 611–616, 1973.

[85] A. Beling and J. C. Campbell, "High-speed photodiodes," *IEEE Journal of Selected Topics in Quantum Electronics*, vol. 20, no. 6, pp. 57–63, 2014.

[86] G. E. Stillman, V. M. Robbins, and N. Tabatabaie, "Iii-v compound semiconductor devices: Optical detectors," *IEEE Transactions on Electron Devices*, vol. 31, no. 11, pp. 1643–1655, 1984.

[87] G. Stillman and C. Wolfe, "Avalanche photodiodes," in *Semiconductors and semimetals*, vol. 12, pp. 291–393, Elsevier, 1977.

[88] L. Components, "T8-t6 thermistor curve." [PDF file], n.d. Accessed: 13-December-2023.

[89] R. Mita and G. Palumbo, "High-speed and compact quenching circuit for single-photon avalanche diodes," *IEEE Transactions on Instrumentation and Measurement*, vol. 57, no. 3, pp. 543–547, 2008.

[90] S. Cova, M. Ghioni, A. Lacaita, C. Samori, and F. Zappa, "Avalanche photodiodes and quenching circuits for single-photon detection," *Applied optics*, vol. 35, no. 12, pp. 1956–1976, 1996.

[91] T. F. Refaat, W. S. Luck Jr, and R. J. DeYoung, "Temperature control of avalanche photodiode using thermoelectric cooler," tech. rep., 1999.

[92] A. Khurana, A. Saxena, and N. Jain, "Evaluation of low power schmitt trigger for communicaion system," *Evaluation*, vol. 2, no. 05, pp. 423–427, 2015.

[93] B. Yerli, C. Eraydin, H. Cinkaya, and K. Durak, "Single photon detection with silicon-based avalanche photodiode," in *Quantum Optics and Photon Counting 2023*, vol. 12570, pp. 110–116, SPIE, 2023.

[94] V. Makarov, "Controlling passively quenched single photon detectors by bright light," *New Journal of Physics*, vol. 11, no. 6, p. 065003, 2009.

[95] I. Prochazka and F. Yang, "Photon counting module for laser time transfer via earth orbiting satellite," *Journal of Modern Optics*, vol. 56, no. 2-3, pp. 253–260, 2009.

[96] I. Prochazka, K. Hamal, and L. Král, "Single photon counting module for space applications," *Journal of Modern Optics*, vol. 54, no. 2-3, pp. 151–161, 2007.

VITA

Burcu Yerli has received her bechelor's degree from the Electronics and Communication Engineering Department at Yildiz Technical University in 2019. She started her Masters' program in the Electrical and Electronics Engineering Department at Ozyegin University with Dr. Durak in 2020. She has been working at TUBITAK BILGEM as a researcher since 2019. She is interested in hardware design, sensing applications, and quantum technologies. Her thesis focuses on single photon detection which is one of the popular quantum applications.